THE FABRICATION OF SILICON CARBIDE HEATING ELEMENTS

by

Zoë G. Smith

A thesis submitted for the degree of Master of Science in Applied Science to the Faculty of Engineering at the University of Cape Town.

Department of Civil Engineering
University of Cape Town

November 1991

THE FABRICATION OF SILICON CARBIDE HEATING ELEMENTS

by

Zoë G. Smith
Department of Civil Engineering
University of Cape Town

November 1991

ABSTRACT

The microstructure of different types of industrially produced heating elements was examined and an x-ray diffraction method was devised to determine the relative amounts of α- and ß-silicon carbide present in these materials. It was confirmed that the α- to ß-silicon carbide transformation occurs during heat treatment, because of the influence of the nitrogen atmosphere in the furnace.

The fabrication parameters important in the manufacture of heating elements were investigated. Porous sintered silicon carbide samples were made using different proportions of grit sizes and various firing schedules. Both resistivity and crushing strength were determined. It was found that the resistivity is dependent upon degree of sintering (indicated by crushing strength) as well as the packing density of the porous body.

CONTENTS

LIST of FIGURES

LIST OF TABLES

1. INTRODUCTION

Silicon carbide is used in many industrial applications because of its high hardness, abrasion, corrosion resistance and high thermal conductivity. The most outstanding properties of this material are at high temperatures, where at temperatures between 1000°C to 1600°C, in either reducing or oxidizing conditions, the strength and creep resistance is still very high in comparison to many other materials. Silicon carbide also has semi-conductor properties.

One of the important applications of silicon carbide is as electrical heating elements. Such products are not manufactured at present in South Africa. In order to understand the factors that influence their properties, different types of commercially available silicon carbide heating elements were analysed, particularly regarding their microstructures. A range of sintered porous silicon carbide bodies were also prepared and analysed to establish how the fabrication parameters affect the resistivity of the material.

2. SILICON CARBIDE

Silicon carbide is very rare in nature. In 1892 Henri Moissan discovered silicon carbide in fragments of the Canyon Diablo meteorite in Arizona and this material was named Moissanite in his honour (Coes, 1971). At the turn of the century Acheson accidently formed silicon carbide while trying to produce diamonds. This method of production is still the major route and is called the Acheson process. The two most common names for industrially produced silicon carbide are Carborundum and Crystolon.

2.1 Polymorphism of silicon carbide

Silicon carbide is polymorphic and crystallizes at atmospheric pressure and room temperature into a diamond lattice (Schwetz, 1989). This basic structure is composed of tetragonal units of silicon and carbon atoms which are held together by strong, highly directional sp^3 hybrid bonds (Whallen, 1986). The bonds in silicon carbide are essentially covalent and, according to Pauling (1960), have 11.5% ionic character.

Although there are about 180 different super-structures of silicon carbide known, all have the same theoretical density of 3.21 g/cc. Thibault (1944) split these polytypes into two categories: the alpha group and the beta group. Alpha (α-) silicon carbide has a hexagonal structure and beta (ß-) silicon carbide has a cubic structure. Later Ramsdell (1947) proposed a new nomenclature system for the several different structures occurring in α-silicon carbide. The number refers to the number of silicon carbide layers in a unit cell, the letter H or R depends on whether the unit cell is hexagonal or rhombohedral. The amounts of the most frequently encountered polytypes 3C (beta-phase), 4H, 15R and 6H (alpha phase), can be quantitatively determined by x-ray diffraction techniques (Schwetz, 1989). Beta silicon carbide occurs in only one cubic form. Table 2.1 relates various types of silicon carbide to Thibault's and Ramsdell's designations. The table shows a selection of the more important polymorphs and does not represent all of the structures known.

Table 2.1: Silicon carbide polymorphs.

Crystal form	Thibault's Designation	Ramsdell's System
Cubic	ß-SiC	ß-SiC
Hex.	III	4H
Hex.	II	6H
Hex.		14H
Rhomb.		15R
Rhomb.	IV	21R
Rhomb.	VI	33R
Rhomb.	V	51R
Hex.		72H
Hex.		408H
Rhomb.		1080R

Although the stability of a given polytype is affected by impurities, amongst other things, it depends mainly upon temperature and this can be used to estimate the temperature of formation. Beta silicon carbide can be formed at temperatures as low as 525°C and it is stable up to 2100°C, at which temperature it slowly begins to transform to alpha silicon carbide. At 2300°C this process is rapid and completed after a few minutes (Baumann, 1952).

The ß- to α- transformation is generally monotropic, but it has also been found that high nitrogen pressure has the effect of enhancing the reverse transformation of α- to ß-phase at a temperature above 2100°C. The greater the pressure of nitrogen the faster the reaction rate. Commonly the transformation is from the cubic 3C ß polytype to the hexagonal 6H α polytype (Jepps, 1981).

2.2 General properties of silicon carbide

In a closed system the decomposition point of silicon carbide has been quoted to be as high as 2735°C, when it breaks down to graphite and silicon. In an open system silicon carbide starts to decompose at about 2300°C with the formation of gaseous silicon and a residue of graphite (Schwetz, 1989). Commercial silicon carbide recrystallises at 2400°C without extensive decomposition. The hardness of silicon carbide is 2480 on the Knoop scale and its theoretical density is 3.21 g/cc (Coes, 1971).

Pure silicon carbide is colourless but industrial grades are coloured from green to black. The different colours are due to the incorporation of foreign atoms in the lattice. Trivalent foreign atoms, namely aluminium or boron, produce a p-type semi-conductor which is blue-black in colour. Pentavalent foreign atoms, mainly nitrogen, produce an n-type semi-conductor which is green.

The heating element industry uses Green Grade silicon carbide which is supplied by various manufacturers. This Green Grade silicon carbide does contain some traces of iron, aluminium and some nitrogen. It is neither a p- or an n-type semi-conductor, but contains a mixture of the two types.

The electrical resistance of silicon carbide can vary within four to five orders of magnitude depending upon the amount of nitrogen in the lattice (Prochazca, 1975). The nitrogen can be incorporated into the lattice by firing in a nitrogen atmosphere. The electrical resistance of silicon carbide varies considerably and non-linearly with working temperature (Forrest et al, 1972), as shown by Figure 2.1.

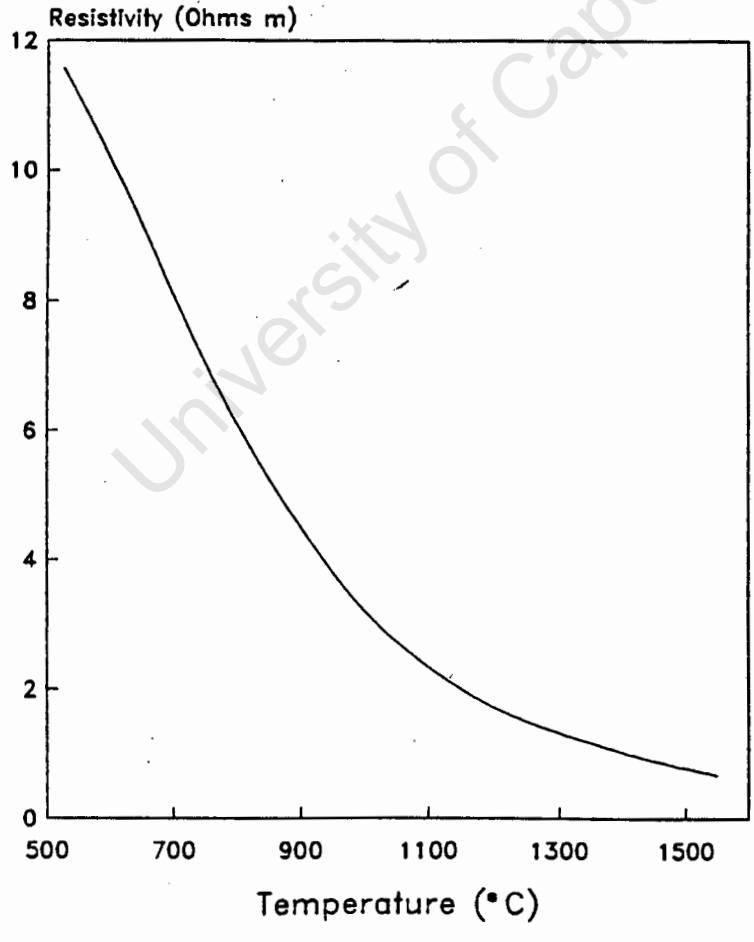

Figure 2.1: Variation of electrical resistivity of silicon carbide with temperature.

2.3 Production of silicon carbide

There are several different methods of producing silicon carbide, depending upon whether α- or ß-silicon carbide is required. To produce α-phase the Acheson process is most commonly used and to produce ß-phase chemical vapour synthesis or the carbothermic reaction is used.

2.3.1 Alpha silicon carbide

The Acheson process is used for the synthesis of silicon carbide from silica and carbon and, although it is the most common source of α-silicon carbide powder, it also produces a large number of different polytypes. The process takes place at temperatures between 1600°C and 2500°C, with the following reactions:

$$SiO_2 + 2C \longleftrightarrow Si + 2CO_{(g)}$$
$$Si + C \longleftrightarrow SiC$$
$$\overline{SiO_2 + 3C \longleftrightarrow SiC + 2CO_{(g)}}$$

The reaction is endothermic, with a heat of formation of 528 KJ/mol. In this process silicon carbide is made from a mixture of salt, sawdust, pure sand and petroleum coke. Petroleum coke is used because it is ash free and therefore has no alumina present. This mixture is heated up to 2400°C in an electric resistance furnace. At this temperature the silica reduces to silicon and the free silicon combines with the coke. The salt assists in removing impurities at high temperatures. The sawdust burns out keeping the mass porous to enable the escape of the carbon monoxide produced by the reactions.

In the old Acheson furnaces carbon monoxide was released into the atmosphere and subsequently a pollution problem arose. Figure 2.2 shows a furnace that was developed by ESK which is ecologically safe (Leithschmidt, 1982). It operates with floor electrodes which enter the reaction mass from below a porous floor. The carbon monoxide is collected by a gas tight plastic canopy and transported through gas collecting pipelines to a power station, where the gases are burned and the energy produced is converted into electrical energy. This power amounts to 20% of the energy requirements of the production process.

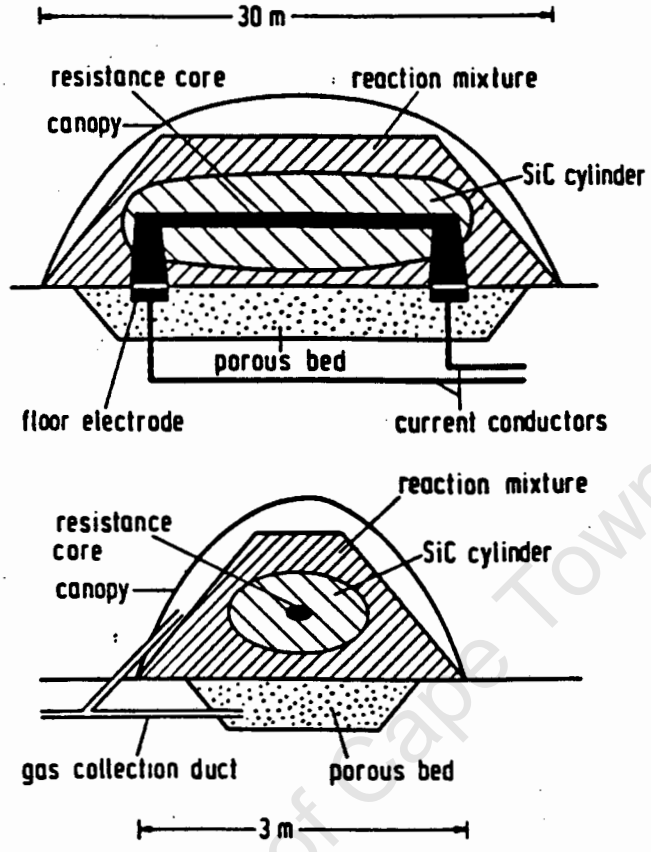

Figure 2.2: Silicon carbide production by the ESK process. Longitudinal and cross sections through the furnace (Leithschmidt, 1982).

The large sintered mass of silicon carbide is jaw crushed, roll crushed and sized. The finest sized powder produced by this method is approximately five microns, which is still too large for sintering purposes. The three methods that can be used to decrease the size of the five micron fraction are ball milling, jet milling and self attrition. As the particle size becomes smaller, milling becomes less effective and the attrition rates become slower. There is also the problem of contamination by the wear of the iron abrading media because silicon carbide is so hard. After milling, the desired size fraction is removed by air or water classification. This is then washed with hydrochloric acid to remove the iron, resulting in an oxide layer forming on the silicon carbide surface. This silica layer can be successfully removed by washing in hydrofluoric acid.

2.3.2 Beta silicon carbide

There are two general methods of producing ß-silicon carbide: chemical vapour synthesis and carbothermic reduction. The quantities of ß-silicon carbide produced in industry are very small, as the demand is greatest for α-silicon carbide.

a. Chemical vapour synthesis

A mixture of a volatile silicon compound, (SiH_4, $SiCl_4$, etc.), a volatile carbon compound, (CH_4, CCl_4, toluene, etc.) and a reducing agent such as hydrogen, perhaps with an auxiliary carrier gas such as argon, is passed through a reactor. In the reaction zone the gases are heated to temperatures over 1000°C to bring about the reaction. Several other options exist, such as silicon and carbon existing within the same volatile molecule (CH_3SiCl_3, CH_3SiH_3, etc.). Low energy efficiency and high materials cost have prevented the vapour process from becoming economically viable as a large scale production method.

b. Carbothermic reduction

Carbothermic reduction involves reacting carbon with silica. This reaction is carried out in a rotary kiln which has a good heat transfer, therefore allowing the temperature to be kept to a minimum. ß-silicon carbide can also be produced by reacting silicon and carbon, but under normal conditions this produces crystalites much larger than those produced via the silica - carbon reaction. The temperature is at approximately 1650°C and the atmosphere is non-oxidizing (Alliegro et al, 1956). It is important to keep the reaction temperature as low as possible to minimize crystal growth, thus preventing the silicon carbide from becoming coarsely crystalline. The product typically consists of weakly bonded agglomerates of small ß-silicon carbide crystalites intermixed with unreacted carbon, crystalline silica and amorphous silica produced by the condensation of the vapour. The agglomerates break down easily during milling and the material can then be treated with hydrofluoric acid to remove excess silicon, while the excess carbon is removed in a floatation cell. Research has found that the material always contains some α-silicon carbide.

3. PRODUCTION OF SILICON CARBIDE PRODUCTS AND THE SINTERING MECHANISMS

Silicon carbide products can be fabricated using either one or a combination of processes. The different types of products are named according to the sintering process they undergo:

Recrystallized SiC
Reaction sintered SiC
Reaction bonded SiC
Sintered SiC
Hot pressed SiC
Hot isostatically pressed SiC
Surface coated SiC

3.1 Sintering mechanisms

Generally there are two types of sintering mechanisms: evaporation-condensation and solid state sintering leading to densification. The mechanisms take place in competition and generally only one is encouraged.

3.1.1 Evaporation-condensation

The evaporation-condensation sintering mechanism in silicon carbide involves the transport of material from an area of high vapour pressure to an area of low vapour pressure. In powder compacts the surface of the grains are convex, while sharp concave surfaces are formed as the contact points between the grains. The difference in the vapour pressures between concave (low pressure) and convex (high pressure) surfaces of the silicon carbide particles is in the order of 10^{-6} to 10^{-5} atmospheres (Kriegesmann, 1986). This pressure difference causes the transport of material from the convex surface of the grains to their contact points, resulting in neck growth between the particles. There is no densification of the powder compact. The following equations represent the reactions that occur:

$$SiO_{2(s)} \; <\text{-----}> \; SiO_{(g)} + 1/2\, O_{2(g)}$$

$$SiC_{(s)} + SiO_{2(g)} \; <\text{-----}> \; 2Si_{(g)} + CO_{(g)}$$

Combining these two equations:

Evaporation ----------> (on convex surface).

$$SiC_{(s)} + SiO_{2(s)} \longleftrightarrow 2Si_{(g)} + CO_{(g)} + 1/2O_{2(g)}$$

Condensation <---------- (on concave surface).

3.1.2 Pressureless sintering

Pure silicon carbide does not densify during pressureless sintering because of the high ratio of grain boundary energy to particle surface energy (Prochazca, 1975). For densification to take place it is necessary for this ratio to exceed a certain critical value, otherwise there is not enough energy available to extend the grain boundaries at the expense of the particle surface area. Sintering aids allow densification to take place either by decreasing the grain boundary energy, or increasing the surface energy.

Pressureless sintering was demonstrated by Prochazca (1974) for ß-silicon carbide and Coppola and McMurtry (1976) for α-silicon carbide. Prochazca (1975) studied the influence of boron and carbon additions on the densification of silicon carbide. Boron and carbon enable the solid to densify because of the effect they have on the ratio of grain boundary energy to particle surface energy. Boron decreases the grain boundary energy due to selective segregation, while carbon increases the particle surface energy by deoxidizing the surface and removing free silicon. Furthermore, in the presence of free carbon the following reaction is possible:

$$SiO_{2(s)} + 3C_{(s)} \longleftrightarrow SiC_{(s)} + 2CO_{(g)}$$

Thus the presence of carbon suppresses the evaporation-condensation mechanism.
To demonstrate the effect different sintering aids have upon the density of silicon carbide, Sunil Dutta (1984) took three types of powder and subjected them to identical sintering conditions: Type 1 powder contained no sintering aids and sintered only to 67% of the theoretical density, while Type 2 powder contained boron and carbon sintering aids and sintered to 96% of theoretical density. Type 3 powder contained aluminium and carbon sintering aids and sintered only to 80% of the theoretical density. In Figure 3.1 densification is plotted against the sintering temperature.

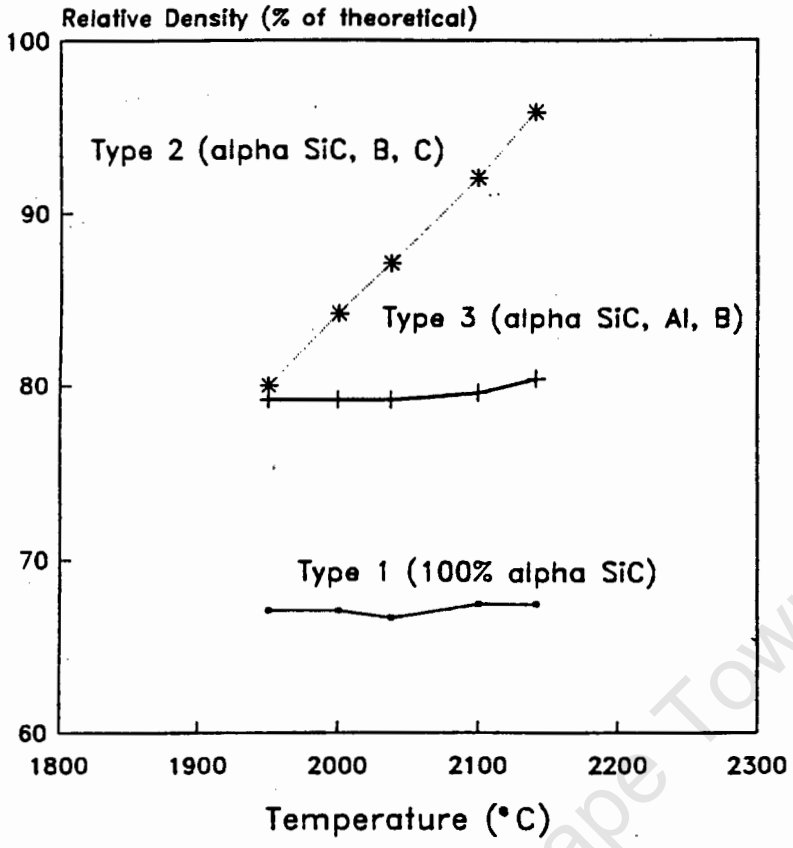

Figure 3.1: Relative density of three types of Starck α-silicon carbide powder sintered for 30 minutes at different temperatures.

Sunil Dutta also found that the material prepared with extra carbon has smaller grains than material that has been prepared without carbon. These findings agree with the results of Prochazca and Charles (1973), who showed that carbon inhibits grain growth. It was Lange and Iskoe (1974) who showed that the strength behavior at elevated temperatures of hot pressed silicon carbide is influenced by the impurity levels of the silicon carbide powders.

3.1.3 Hot pressing

Pure silicon carbide can be densified at temperatures above 2000°C and pressures greater than 2000 MPa without the use of sintering aids (Nadeau, 1973), but at lower temperatures and pressures sintering aids are required. For example, with uniaxial hot pressing with graphite tools it is still necessary to use small amounts of sintering aids because the pressure used is not enough to decrease the ratio of grain-boundary energy to particle surface energy.

The evaporation-condensation sintering mechanism does not take place as the high pressure opposes evaporation. Densification could be enhanced further via particle rearrangement or plastic flow (Bind et al, 1975). Watson et al (1985) concluded that the densification obtained by hot isostatic pressing is due to the elimination and/or reduction of the pores, but not due to compression of the gases within the pores.

3.2 Fabrication

3.2.1 Recrystallized silicon carbide

Recrystallized silicon carbide is a porous material. The pores are interconnected and constitute approximately 20% of the structure. The density of recrystallized silicon carbide is approximately 2.66 g/cc and its strength is about 90 MPa (Kriegesmann, 1986).

The sintering mechanism is evaporation-condensation. There is no shrinkage during sintering, which makes it possible for large components to be manufactured with good dimensional accuracy, thus requiring no machining.

The α-silicon carbide powders used in the fabrication of recrystallized silicon carbide have a bimodal grain size distribution. The coarse grains have an average grain size of 25 microns and the finer grains range from submicron to 10 microns while the mass ratio of coarse to fine grain fractions is generally 70:30 (Kriegesmann, 1988). The coarse grains lie in contact with one another and the smaller grains lie in between. This mixture is either slip cast or press moulded to produce a material of high green density. The compact is fired in an electric furnace at temperatures up to 2500°C in an inert atmosphere, usually nitrogen, and without sintering additives. Firing in a nitrogen atmosphere promotes the conversion of α-silicon carbide to ß-silicon carbide (Jepps, 1981).

3.2.2 Reaction bonded silicon carbide

Reaction bonded silicon carbide is produced by bonding α-silicon carbide particles with ß-silicon carbide, which are formed *in situ* by the reaction of carbon and silicon. Carbon, α-silicon carbide and organic binders are mixed, compacted and then heated in air to remove the binder. After firing the compact consists only of carbon and silicon carbide which is subsequently green machined. The machined parts are then placed above a silicon billet in a vacuum induction furnace and heated to about 1600°C. As the silicon melts at 1410°C it infiltrates the compact and reacts with the graphite to form ß-silicon carbide. This newly formed ß-silicon carbide bonds the original α-grains together (Forrest at al, 1972). The porosity of the initial compact must permit complete silicon impregnation, and provided that the porosity in the initial compact is correct, bodies of zero porosity can be obtained. There are no dimensional changes occurring during the reaction bonding process and bodies can be fabricated to close dimensional tolerances.

An alternative production method is to include the correct amount of silicon powder in the powder mix before compacting and heating to the reaction temperature. As the silicon sweeps up by capillary action through the compact, it carries impurities from the carbon and silicon along with it, concentrating them as it progresses. After firing, the impurity-laden silicon on the surface is removed by blasting with alumina grit and the part is then machined to the desired surface finish (Forrest et al, 1972 and Ness and Page, 1986).

The silicon content of different grades can range from 5% to 20%, but it is generally recognized that a silicon content of 12% or less is preferred for chemically aggressive environments (Lashway et al, 1984). The grain structure and silicon-filled pores must be fine and evenly distributed throughout the material. Unfortunately at temperatures above 1200°C sweating out occurs and the creep rate becomes increasingly large as the working temperature is increased (Whallen, 1986).

3.2.3 Reaction sintered silicon carbide

Reaction sintered silicon carbide is fabricated by the same method as reaction bonded silicon carbide, but it contains some free silicon and some free carbon as second phases (Wu et al, 1985).

These materials have essentially zero porosity and are designed to enhance the tribological properties of the conventional silicon carbides (Berroth, 1990). However, the abrasion resistance is not as good as that of surface coated silicon carbide (see section 3.2.7) because of the presence of free graphite within the structure. The variation in grain size is in the range of 10 - 1000 microns and the carbon content in the range of 5 - 20%. Reaction sintered silicon carbide is expensive and difficult to manufacture.

3.2.4 Sintered silicon carbide

Sintered silicon carbide is produced from a blend of α-silicon carbide grit, sintering aids and binders. The most common sintering aids are 1 to 2 mass % of boron or aluminium. The mix must also contain an additional 1 to 2 mass % of free carbon to suppress the evaporation-condensation mechanism. The compact is sintered, without any application of pressure, at 1800-2200°C in an inert atmosphere or in a vacuum (Lashway et al, 1984). Densification takes place as described in sections 3.1.2.

The linear shrinkage is high (18% or more) and the compact contains only closed pores. The density exceeds 98% of the theoretical density, while the strength of sintered silicon carbide can be as high as five times that of recrystallized silicon carbide.

3.2.5 Hot pressed silicon carbide

The importance of hot pressed silicon carbide has probably decreased slightly since the development of pressureless sintered silicon carbide. However, it is currently still the most suitable method of obtaining silicon carbide with the best mechanical properties, even though it is expensive and therefore only used where high strength requirements make its use imperative. Unfortunately precision parts can only be produced by machining with diamond tools which is expensive. The maximum pressure of hot pressing is 50 MPa, which is limited by the strength of the graphite die. The atmosphere is either neutral or a vacuum and the sintering temperature is between 1900°C and 2000°C.

Figure 3.2 shows the density of the silicon carbide as a function of hot pressing temperature, type of silicon carbide grit and type of sintering aids. The most efficient sintering aids were found to be aluminium (or Al_2O_3) and iron. These give relative densities greater than 98% at temperatures less than 2000°C and pressures as low as 40 MPa (Alliegro et al, 1956). Addition of carbon to suppress evaporation-condensation is not necessary because of the high pressures used.

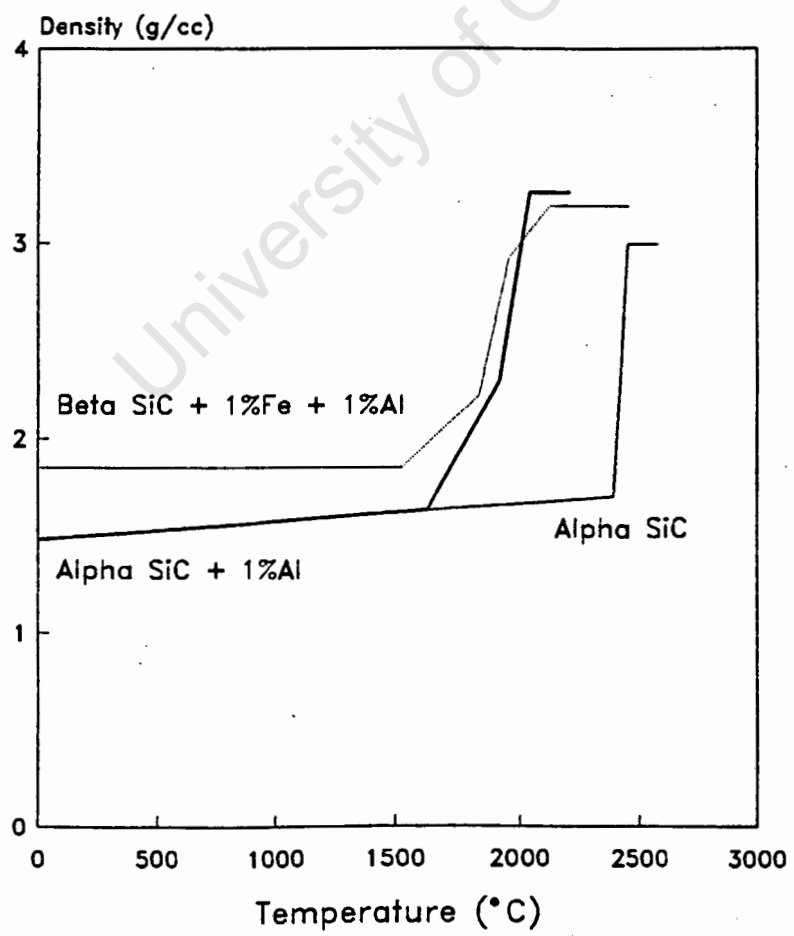

Figure 3.2: Density of silicon carbide as a function of hot pressing temperature.

3.2.6 Hot isostatic pressing

A more expensive method than conventional hot pressing, is hot-isostatic pressing (HIP). In hot isostatic pressing both high temperature and high pressure are used simultaneously in the fabrication process. Usually pressureless sintered silicon carbide is the starting material and the amount of pressure applied is dependent upon whether sintering aids are used. Today pressureless sintering and isostatic hot pressing can be performed in the same cycle. This new process is called "sinter HIP" and offers economic benefits.

Densities can be improved from 97%, achieved by pressureless sintering, to over 99% of the theoretical density by cladless hot isostatic pressing at about 2000°C. Watson and co-workers found that hot isostatic pressing increases the strength at room temperature and at 1200°C, resulting in improved reliability. Grain size was also observed to increase with increasing hot isostatic pressing temperature (Watson et al, 1985). Isostatically hot pressed α-silicon carbide exhibits an ultra-fine grained microstructure of 0.3 to 3 microns, compared to grain sizes of 1 to 17 microns produced by sintering (Sunil Dutta, 1988).

3.2.7 Surface coated silicon carbide (siliconized carbon)

The siliconized graphite family represents the coated SiC group (Lashway et al, 1984). According to the ESK 1988 publication, siliconized carbon is produced by exposing a porous carbon substrate to silicon vapour at high temperatures, which diffuses into the substrate and reacts with the carbon to form silicon carbide. A surface layer approximately 0.5 mm thick is formed, preventing further diffusion of silicon into the base material. Forrest, Kennedy and Shennan (1972) exposed a porous carbon matrix to a silicon monoxide atmosphere. The silicon monoxide seeped into the matrix and converted the graphite on the surface to silicon carbide leaving approximately 10% free graphite, forming a layer approximately 1-2 mm thick. The material was subsequently impregnated with resin to make it impervious to water.

Surface coated silicon carbide is very fragile because the core material is porous graphite. Siliconized graphite is mainly used for industrial pump seals, but it is not generally used in chemical or refinery seal applications. The silicon carbide layer should be in excess of 2 mm thick since the base graphite is extremely soft.

Unfortunately the resin imposes limitations on chemical and temperature resistance. Components can be machined in the graphite form before conversion, enabling complicated shapes to be produced more economically than by other fabrication techniques.

4. EXPERIMENTAL TECHNIQUES

4.1 Investigation of industrial samples

4.1.1 Optical microscopy

The specimens were mounted in Buehler Transoptic powder, using a Metaserv mounting press. Initially, before a diamond grinding wheel was obtained, rough grinding was carried out on water lubricated bonded silicon carbide papers on a rotating wheel, starting with 80 grit paper and progressively working through to 600 grit, with grinding times increasing from 5 minutes to 30 minutes per grade. A weight of 2 kg was used to hold the sample in position on the paper. Every few minutes the sample was moved to a new track and the sample rotated through 90°. At a later stage a diamond wheel was obtained for use with a Jones and Shipman surface grinding machine. The specimens were passed under the wheel three times, after which the samples were ground on a 600 grit paper for 30 minutes.

Polishing was performed on a series of diamond impregnated Buehler polishing cloths with Buehler Automet lapping oil. Initial polishing was carried out with 15 micron diamond paste, followed by 7 micron and 3 micron and finally by 0.25 micron paste. Polishing time was 6 hours for every grade of diamond paste. The specimens were thoroughly cleaned ultrasonically in ethanol between each grade of paste.

A number of etching procedures (Clinton, 1987) were tried with varying degrees of success. The following etching treatments failed:

a. Electrolytic etch, using CrO_3 and H_2SO_4 in equal parts of acetic acid and water.
b. HF and concentrated nitric acid at 25°C.
c. Molten KOH for 8 minutes.
d. Electrolytic etch, in 20% KOH at 6V, 1A for 20 seconds.

The etching procedure that proved to be more successful and which gave the best results was as follows: The specimen surface was covered with Murakami's etchant and boiled to dryness. The recipe for Murakami's etchant is 10g NaOH, 10g $K_3Fe(CN)_6$ and 100ml H_2O.

Micrographs were recorded on a Nikon Polarizing Microscope using an automatic camera system and Ilford FP4 film of 125 ASA.

4.1.2 Scanning electron microscopy

Polished, etched and fracture samples were sputter coated with Au-Pd for normal imaging. Scanning electron micrographs were recorded using the Cambridge S180 Stereoscan system of the Electron Microscopy Unit at the University of Cape Town. The micrographs were taken using 120 mm Ilford FP4 film of 125 ASA. At a later stage the Electron Microscope in the DeBeers Research Laboratories was used. The film used for those micrographs was Polaroid.

4.1.3 Estimation of the percentage of Á-silicon carbide in commercial heating elements

A comprehensive description of the quantitative x-ray diffraction method used to determine the amount of α- or ß-phase present in the silicon carbide materials are given in the Appendix.

The samples were milled for three minutes in a Siebtechnik crushing mill. The x-ray diffraction conditions used for the analysis of each sample are given in the appendix and the diffraction traces are shown in Figures 4.1 to 4.5. The d-spacings (in Å) of the peaks are also given in the figures.

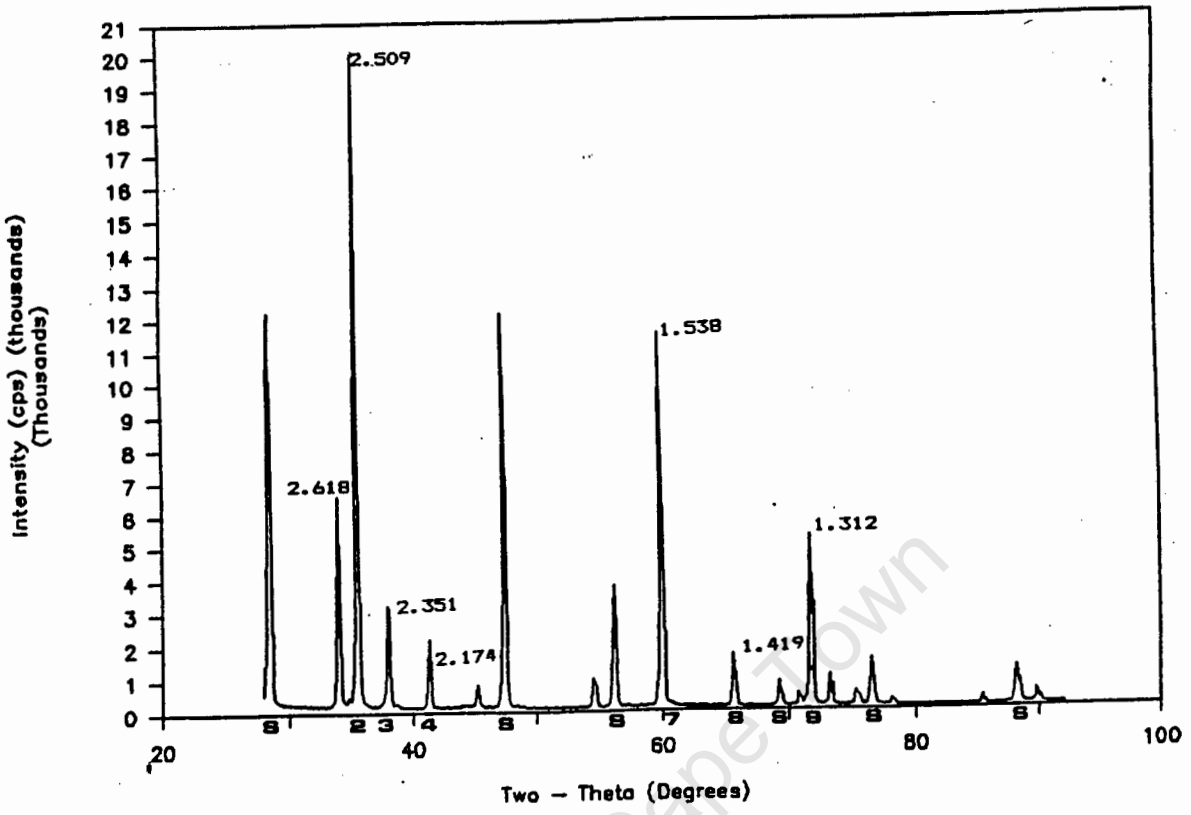

Figure 4.1: X-ray diffraction trace: Cold section of the Kanthal Hot Rod heating element.

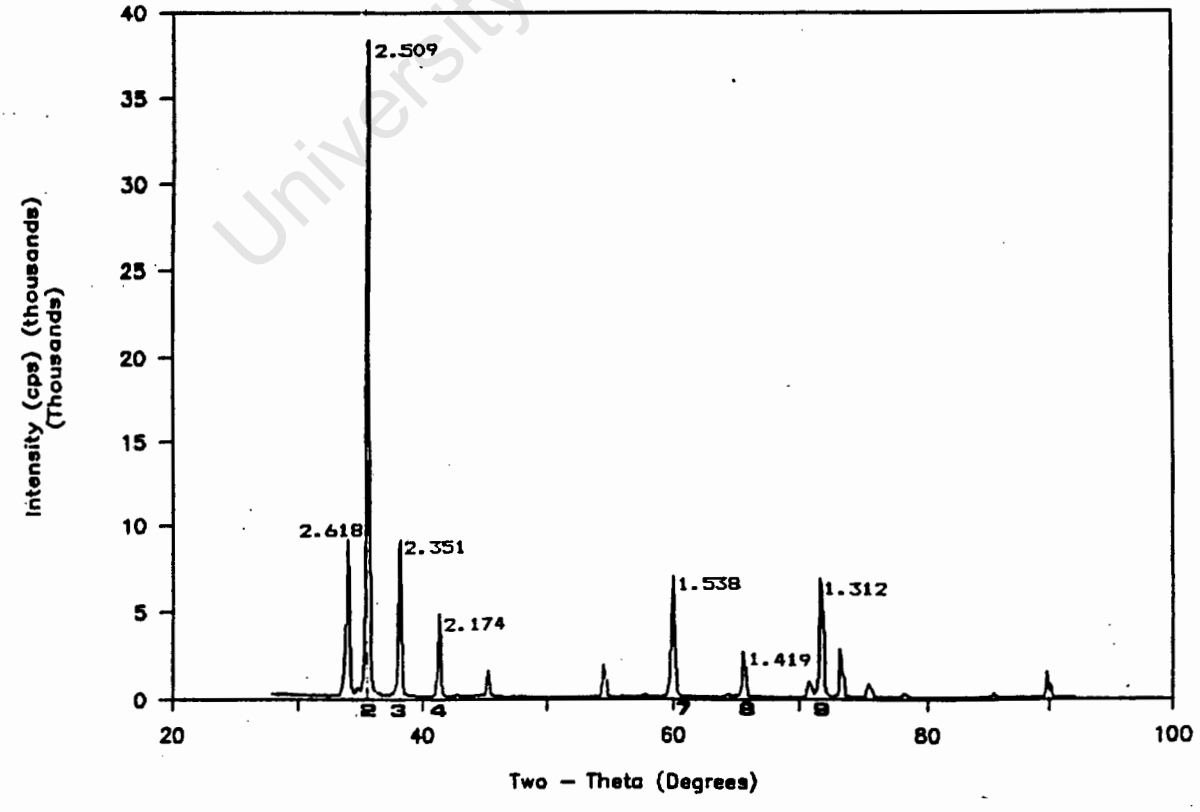

Figure 4.2: X-ray diffraction trace: Hot section of the Kanthal Hot Rod heating element.

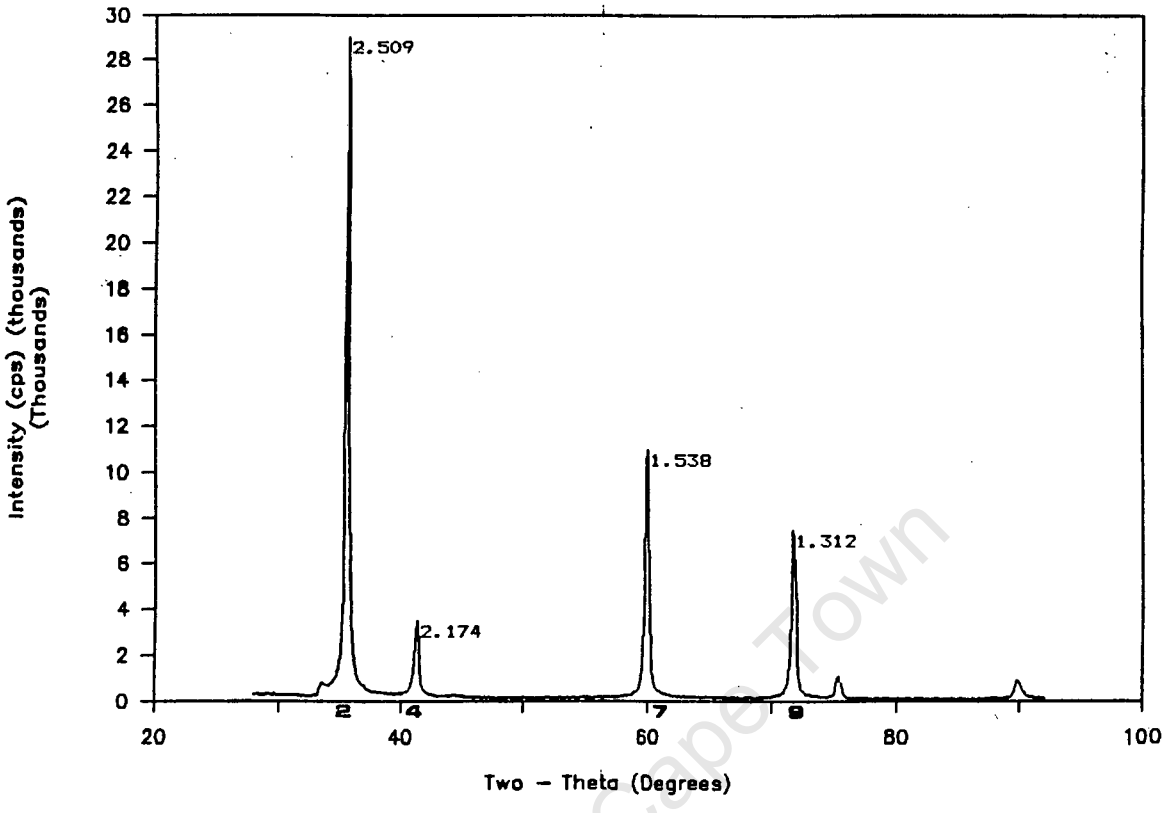

Figure 4.3: X-ray diffraction trace: Hot and cold section of the Kanthal Crusilite heating element.

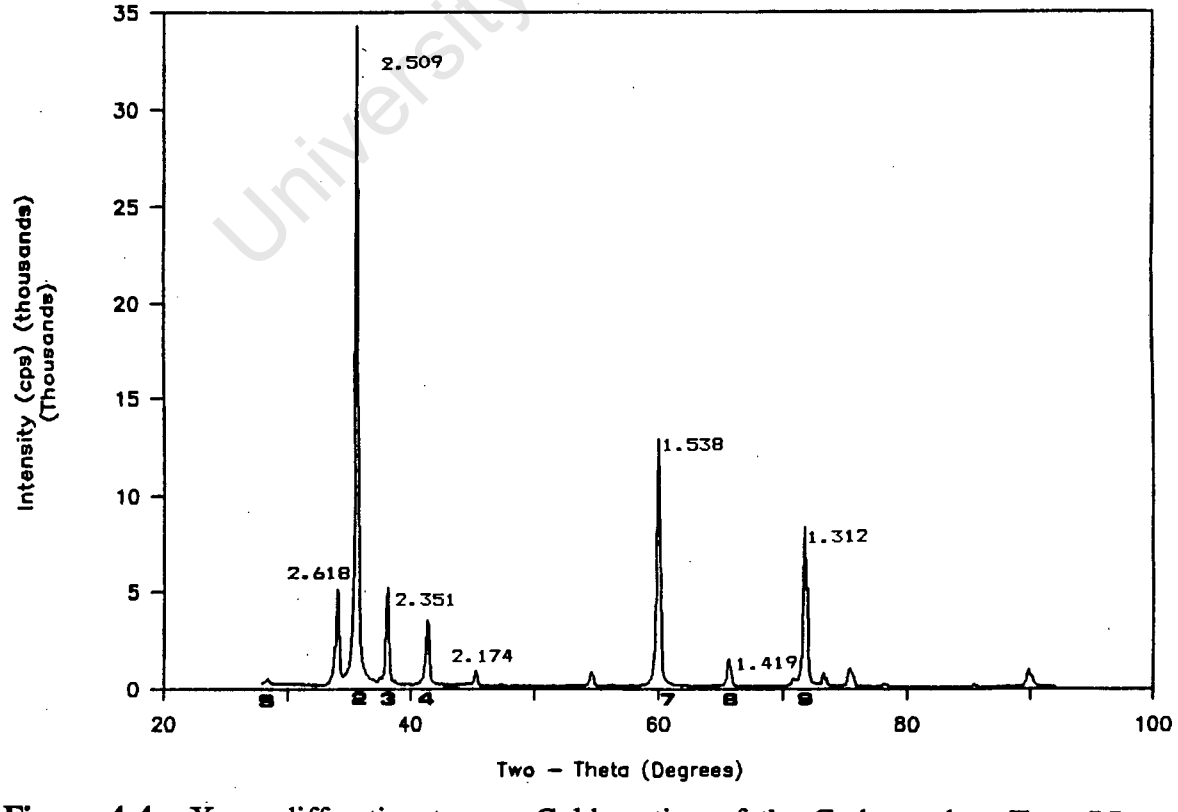

Figure 4.4: X-ray diffraction trace: Cold section of the Carborundum Type LL heating element.

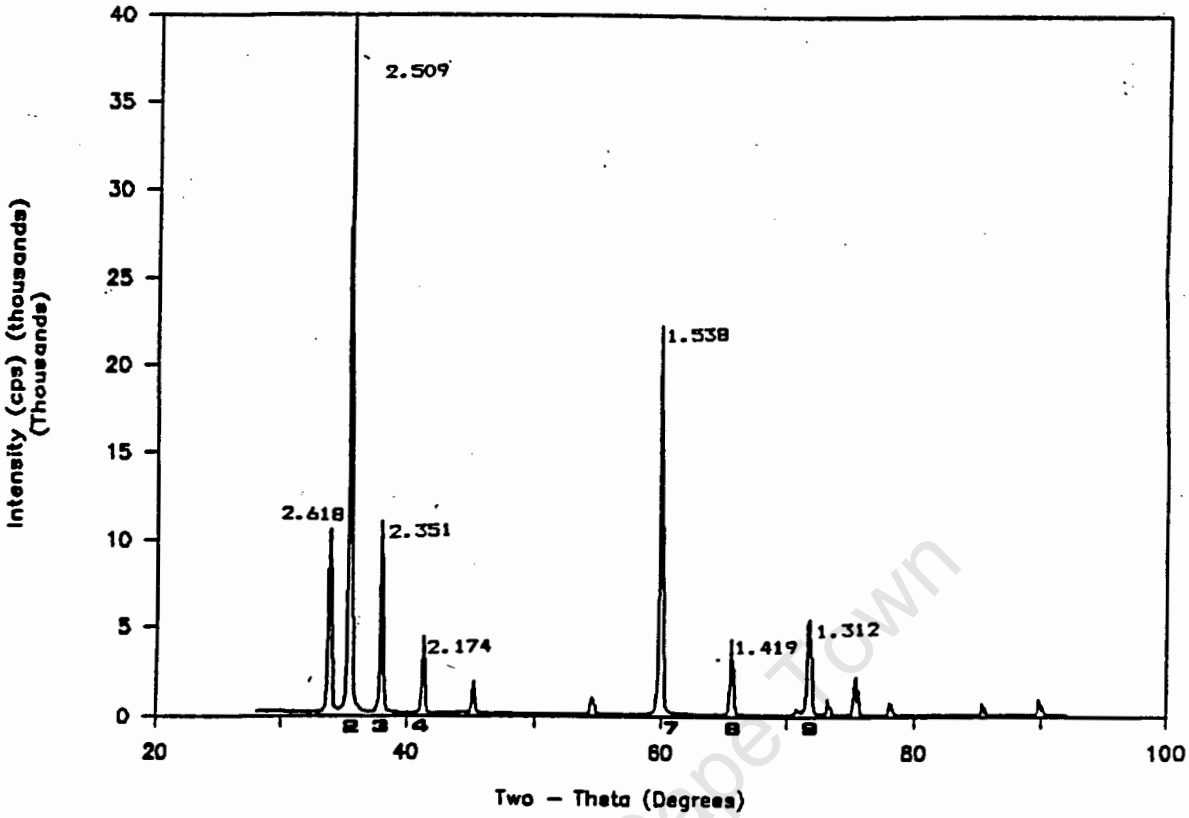

Figure 4.5: X-ray diffraction trace: Hot section of the Carborundum Type LL heating element.

For the reasons given in the appendix, the intensity ratio used for determining the amount of α- and ß-phase present in the samples was:

$$\text{Intensity Ratio} = \frac{\text{Peak 3 - Peak 4}}{\text{Peak 4}}$$

The net intensities for peaks 3 and 4 were determined from the x-ray diffractometer printout and the Intensity Ratio calculated. The values found for each sample are given in Table 4.1.

Table 4.1: The % of α-SiC (% ß-SiC = 100 - % α-SiC) calculated from the Intensity Ratio of the different heating elements.

Heating Element	Ratio 1	Ln((Ratio 1) + 2))	% of α-SiC
Kanthal Hot Rod hot section: cold section:	 1,2573 0,9900	 1,1809 1,0953	 80,5%±2,5 74,7%±2,5
Kanthal Crusilite:	-1,1664	-0,1820	0
Carborundum Type LL hot section: cold section:	 1,7344 0,2023	 1,3176 0,7895	 90,2%±2,5 53,5%±2,5

The cold sections of the Carborundum heating element and the Kanthal Hot Rod contain free silicon. The x-ray diffraction trace for pure silicon (high purity standard reference silicon SRM640A obtained from the Bureau of Standards in the USA) shown in Figure 4.6 shows that the peaks do not overlap the α- or ß-SiC peaks. The silicon peaks are marked with an "s" on the traces of the heating elements.

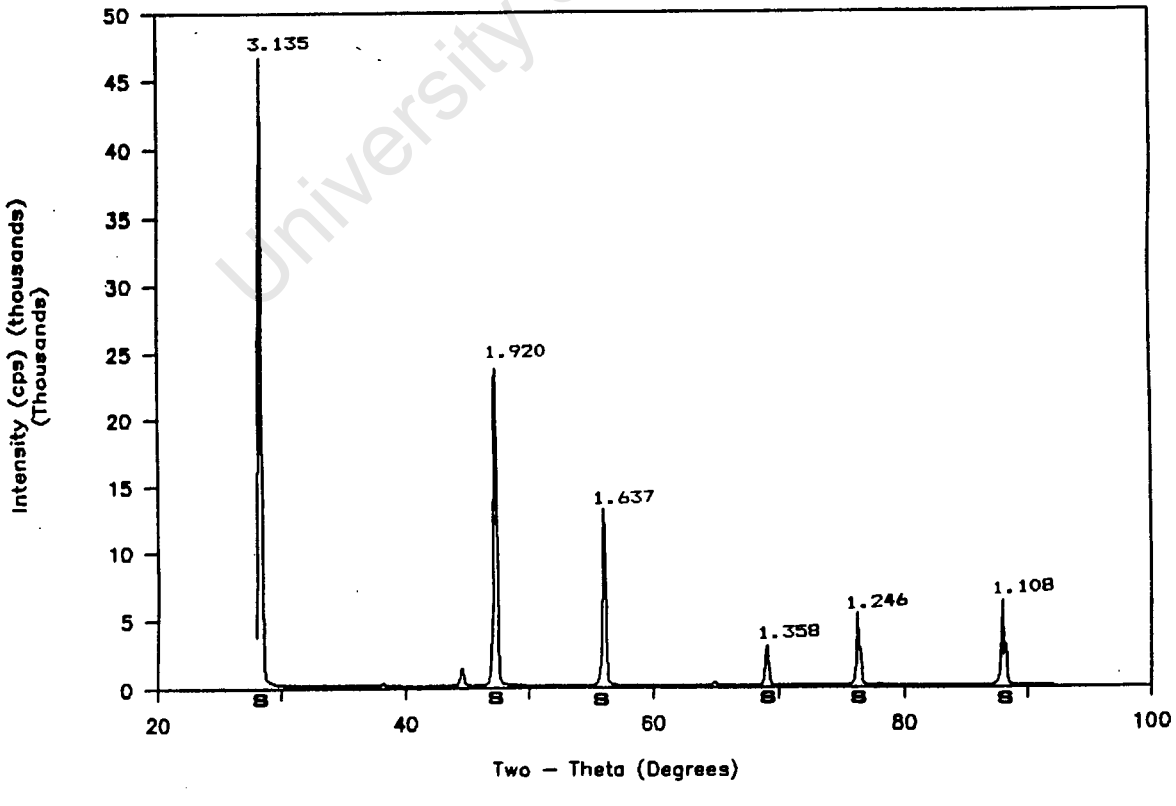

Figure 4.6: X-ray diffraction trace: pure silicon.

The amount of free silicon was calculated using the two strongest peaks located at a d-spacing of 3,135 Å and 1,920 Å. Peak intensities were calculated between angles 28° to 29,6° and 46,5° to 47,9°. For the Kanthal cold section the amount of free silicon was found to be approximately 45%. The trace amount of silicon present in the cold section of the Carborundum Type LL heating element was too small to be measured sensibly by x-ray diffraction.

4.2 Preparation of experimental bodies

4.2.1 Analysis of the silicon carbide grit

Four different grit sizes of Green Grade silicon carbide were obtained from Cumar Abrasives (Springs, Tvl.) namely F90, F180, F240 and F600. An ultra fine grit, A10, was also obtained from Hermann C. Starck in Berlin (see also Appendix A1.2).

The grits were analysed with a Malvern particle size analyzer, using a focal length of 300 mm. Table 4.7 compares the Malvern results with the specifications of the manufacturers. The Malvern results report the average size (50% <) and the size that 90% of the grit is smaller than (90% <).

Table 4.2: Particle size analysis results from the Malvern and the particle sizes specified by the manufacturers.

Grit type	Manufacturers size spec. (50% <)(micron)	Malvern (micron) 50% <	90% <
F90	180-125	215	332
F180	90-53	106	157
F240	42.5-46.5	59	95
F600	8-10	15	26
A10	max. 0.8	1.4	2.1
Alumina		1.8	3.0
Silica		15.5	37.5

4.2.2 Compounding of mixes

Porous silicon carbide bodies are generally compounded of coarse and fine grits in the proportions of 70:30 (Kriegesmann, 1988). Nine mixes were prepared, using the various grits in the proportions given in Table 4.8. To each mix of 2.48 kg 82.7 g of alumina and 82.7 g silica was added. Also added was 68.9 ml of polyethylene glycol (PEG 400) and 100 ml of water. Both the alumina and the silica was supplied by Debex (Pty) Ltd and the PEG 400 was supplied by Chemical Small Pak, Springs.

Table 4.3: Proportions of silicon carbide grits used in each mix.

Mix	Coarse grit	Fine grit
	F90	**F600**
Mix 1	80%	20%
Mix 2	70%	30%
Mix 3	60%	40%
	F180	**F600**
Mix 4	80%	20%
Mix 5	70%	30%
Mix 6	60%	40%
	F240	**A10**
Mix 7	80%	20%
Mix 8	70%	30%
Mix 9	60%	40%

From each mix 210 grams were measured out and compacted uniaxially in a Bencor press at a pressure of 7.5 tons. The billets were then dried in a cyclone oven for 2 hours at a maximum temperature of 400°C. Each sample was weighed and measured so that the pre-sintered densities could be calculated.

4.2.3 Sintering of the billets

A billet from each mix was sintered in an unpressured Harper furnace in a nitrogen atmosphere. They were pushed through the furnace at a rate of 0.65, 0.80, and 1.44 m/hour. The length of the hot zone was 1.5 m, thus the times in the hot zone were 2 hr 18.5 minutes, 1 hr 52.5 minutes and 1 hr 2.5 minutes respectively. The sintering temperatures used for this study were 2000°C, 2200°C and 2400°C.

To ensure that the surfaces of the samples are flat and parallel for the resistance measurements, they were ground using a stone wheel with water lubrication on a

Jones and Shipman grinding machine. The samples were then dried in an oven at 45°C for 48 hours to remove any water that may have been absorbed during grinding.

4.3 Measurement of resistivity at high temperature

4.3.1 Resistivity rig

A rig to measure resistivity at high temperature was designed and constructed. The specimens themselves formed the resistance element in an electrical heating circuit and by controlling the voltage the specimens could be heated at any desired rate. The resistivity at any temperature could be calculated from measurements of the volts and amps at that moment. Figure 4.7 shows the design of the rig, while Figure 4.8 shows the electrical circuit used.

The conducting rods that held the specimen in position were the cold ends of a Kanthal Hot Rod heating element. The contact area of these rods was smaller than the billet, making it necessary for conductive graphite discs, 1 mm thick, to be placed between the two contacts. The graphite discs ensured that the current passed through the full surface area of the billet. To ensure a good electrical contact between the billet, the graphite discs and the rods the billets were painted with a colloidal graphite paint. Graphite powder was also sprinkled between the billet and the disc and between the disc and the rods.

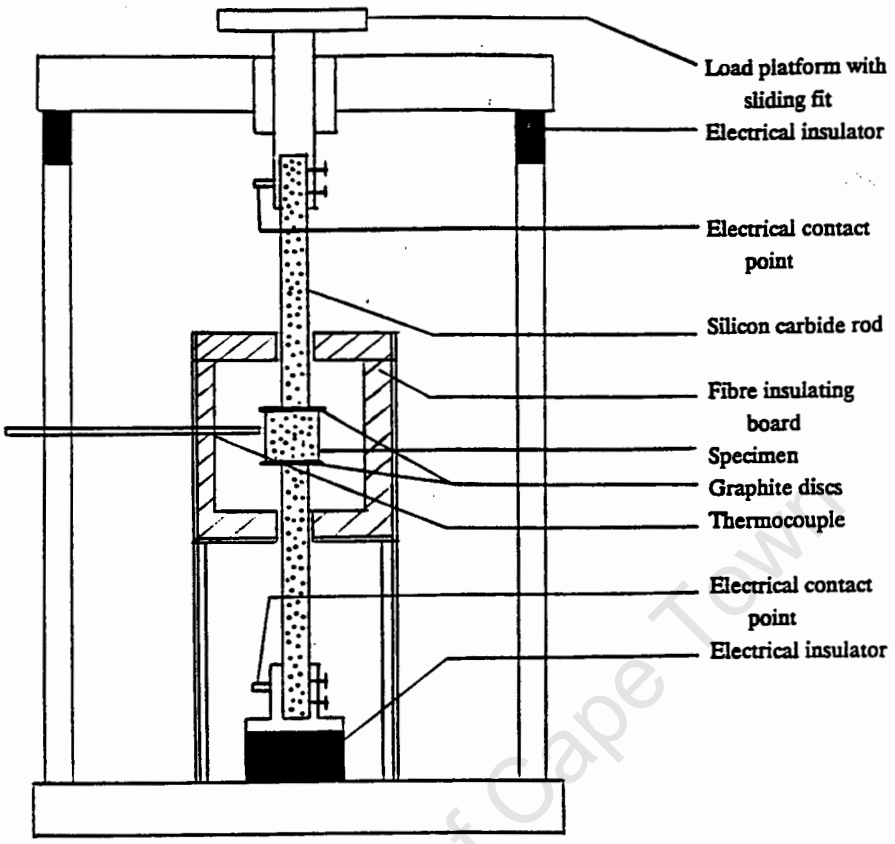

Figure 4.7: Apparatus used to measure the resistance of a sample with increasing temperature.

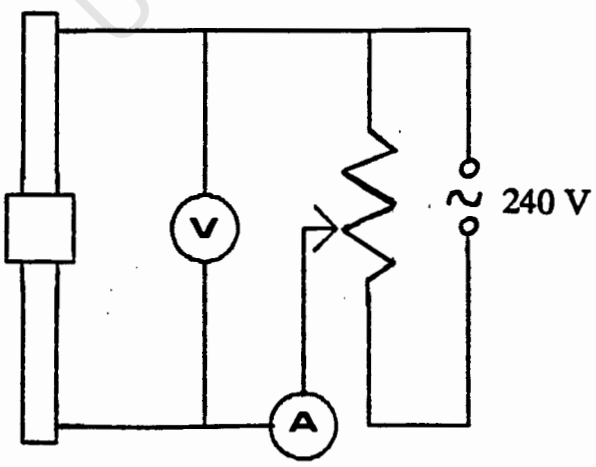

Figure 4.8: Electrical circuit used to measure the resistance of a sample with increasing temperature.

A Variac was used to control the voltage that is passed through the billet. As the temperature increased, the volts and amps were noted and, using Ohm's law: V = I R, the resistance at that temperature was calculated. From the measurements of the specimen dimensions the resistivity of each billet was obtained:

$$R = \frac{r\,l}{A}$$

Where: R = Measured resistance (Ω)
r = Resistivity (Ωm)
l = Length (m)
A = Area (m^2)

The rig was designed to operate at a maximum voltage of 240 V and a maximum current of 40 Amps. Care was needed to avoid a runaway of the current, particularly during the starting period. The temperature of the billet was measured with a platinum thermocouple. Graphs of resistivity vs temperature were then plotted. Kanthal (1989) reports that there is a definite inflection in the resistivity at about 800°C, after which the resistance of the heating elements starts to increase slowly with increasing working temperature. Although such an inflection was not observed in this study, the resistivity values at 800°C were used for comparison.

4.3.2 Reproducibility of resistivity measurements

To test the reproducibility of the resistivity measurements, a billet was rerun on the apparatus 5 times. Figure 4.9 shows the results obtained on a billet from Mix 8 that had been fired at 2000°C at a furnace track rate of 0.80 m/hr. The average value of resistivity at 800°C was 0.987 Ωm, with a standard deviation of 0.0135 Ωm.

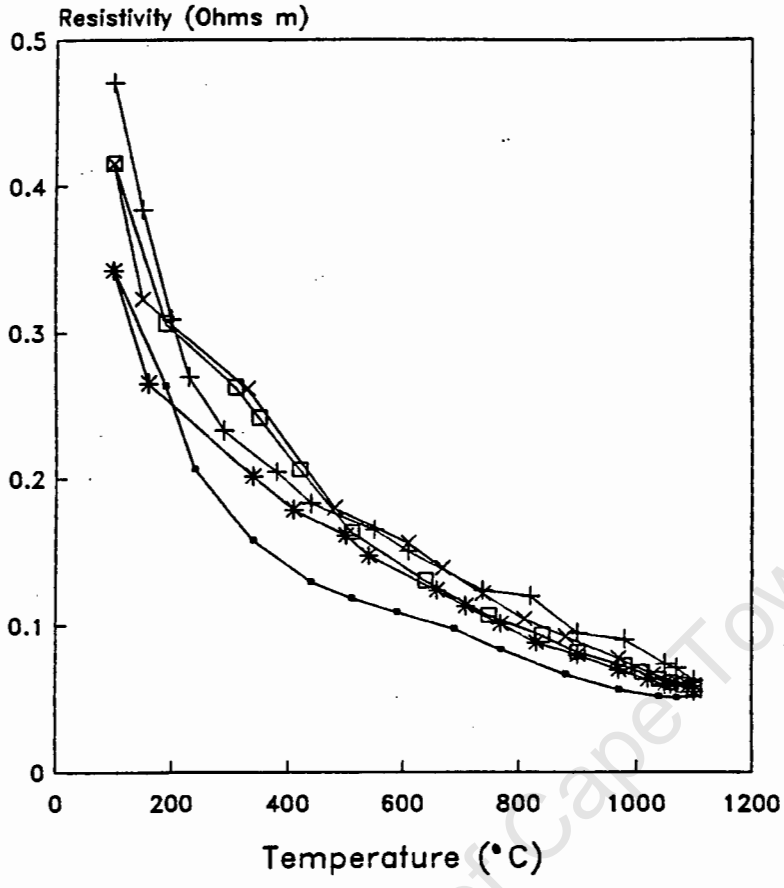

Figure 4.9: Repeat measurements of resistivity vs temperature for a billet from Mix 8, fired at a temperature of 2000°C, at a furnace track rate of 0.80 m/hr.

4.4 Crushing strength tests

The crushing strength of each specimen was measured with an Instron testing machine. A piece of thick card was placed between the surfaces of the platens and the billet to ensure a fair contact. The final pressure required to cause the sample to fail was recorded.

5. MICROSTRUCTURAL STUDY OF INDUSTRIAL HEATING ELEMENTS

Three types of heating elements were acquired for detailed microstructural analysis. These heating elements were Kanthal Hot Rod, Kanthal Crusilite and Carborundum Type LL heating element. The objective of the analysis was to understand the characteristic microstructural features that develops as a result of the manufacturing methods used in the production of silicon carbide heating elements.

Three different types of heating elements, in a variety of styles, are manufactured. Each heating element consists of hot and cold sections. A power source is attached to the cold sections which extend through the furnace walls, while the hot section inside the furnace generates heat in direct proportion to the amount of power supplied. The cold sections remain cool because their electrical resistance is considerably lower than the hot section; the ratio of the resistance between the sections is approximately 25:1. Figure 5.1 shows some of the styles of heating elements that are available.

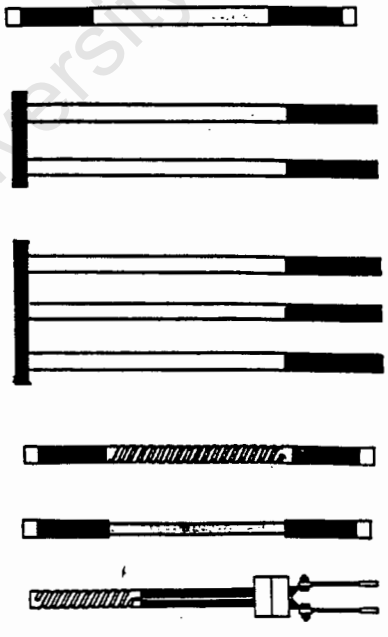

Figure 5.1: Different types and styles of heating elements. The dark coloured portions are the cold sections.

5.1 Type 1: Kanthal Hot Rod heating element

The heating element is manufactured as a single unit. A blend of α-silicon carbide, with a range of grit sizes, is mixed with a binder. The rod is made by either extruding the mix or packing it into cardboard tubes. The rods are then sintered in a nitrogen atmosphere at temperatures above 2200°C for approximately an hour. The sintering mechanism is evaporation-condensation. The cold sections are manufactured by immersing the ends of the element into molten silicon at approximately 2100°C. Because silicon wets the surface of silicon carbide, it will infiltrate effectively, thus filling the pores completely and producing a dense material with a low electrical resistance.

5.1.1 Cold section

Figure 5.2 is a micrograph of an unetched polished specimen of the cold section of a Kanthal Hot Rod heating element. The lighter areas are silicon and the dark grey areas are silicon carbide. The average intercept length of the silicon carbide grains is 0,17 mm and of the silicon infiltrated areas 0.10 mm. Lineal image analysis found the proportion of silicon to be 51.9% of the total volume, which compares well with the value of 44.8% silicon found to be present by x-ray diffraction.

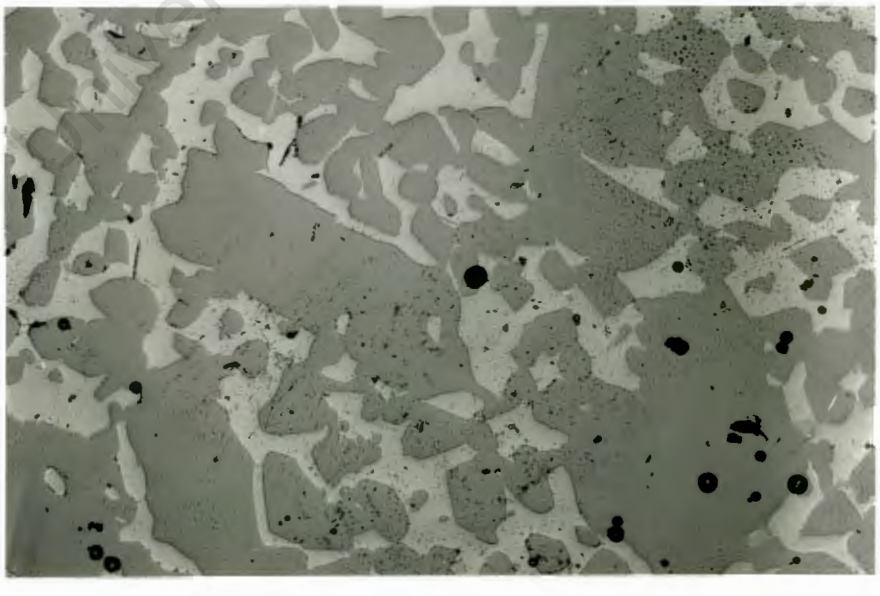

Figure 5.2: Kanthal Hot Rod heating element, cold section, unetched polished specimen. Magnification = 50X.

Figure 5.3 shows the microstructure of the cold section after etching with Murakami's agent. The etching revealed an interesting microstructural feature. All the silicon carbide grains appear to consist of two concentric phases, with the boundary between the phases very clearly demarcated. Lineal image analysis yielded a ratio of 63% to 37% for the volume of the center or core phase to the volume of the outside or surface phase.

From an x-ray diffraction analysis it was estimated that the amount of α-silicon carbide present in the silicon carbide grains is 74,7% (± 2.5%); the amount ß-silicon carbide is thus 25,3% (± 2,5%).

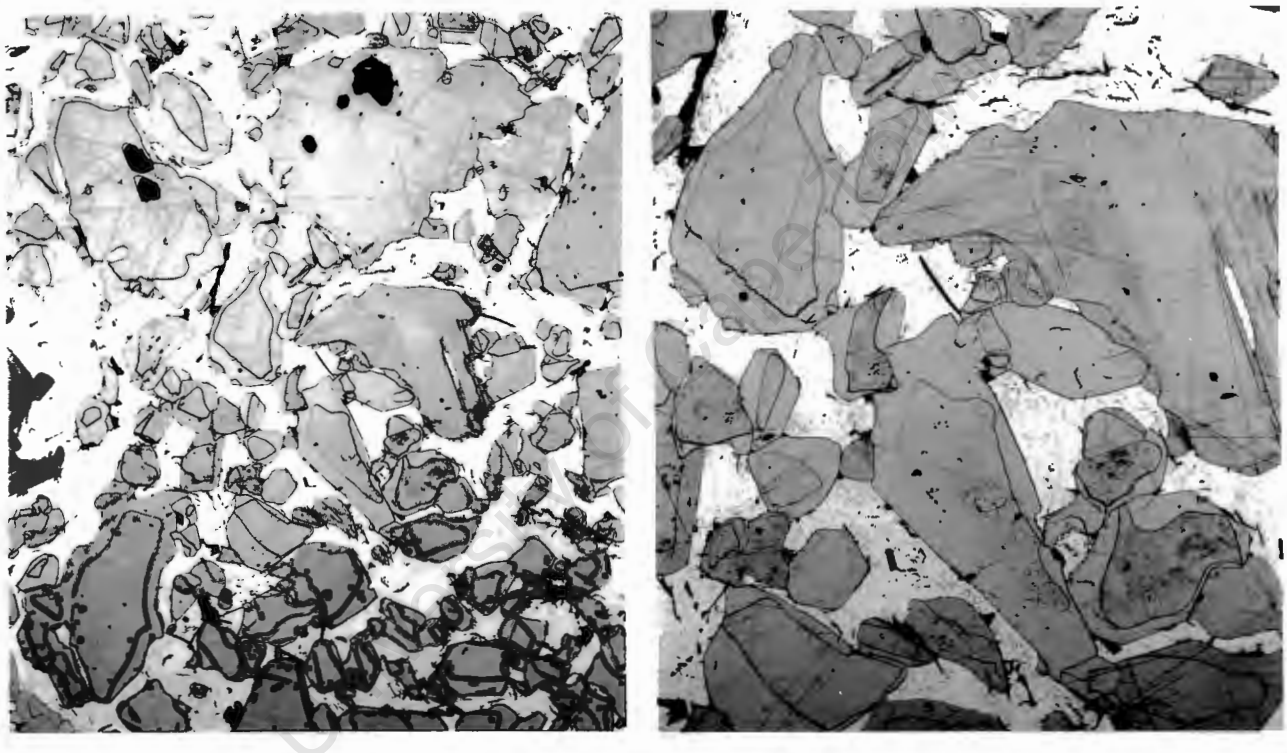

Figure 5.3: Kanthal Hot Rod heating element, cold section, etched polished specimen. Magnification = 50X and 110X.

Figure 5.4 is a scanning electron micrograph of an etched polished specimen of the cold section. The micrograph shows that the core or center areas of the silicon carbide grains have been preferentially attacked. Murakami's agent is known to etch α-silicon carbide faster than ß-silicon carbide (Heuer et al, 1978), thus it was deduced that the cores of the grains consist of α-silicon carbide and the surface phase of ß-silicon carbide. This conclusion is supported by the other two determinations, ie. lineal image analysis and XRD analysis.

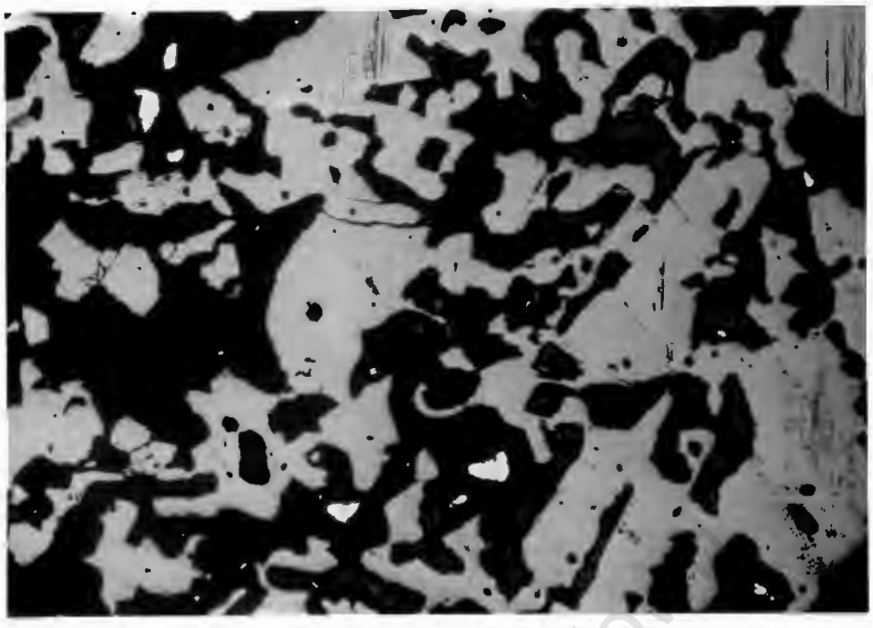

Figure 5.5: Kanthal Hot Rod heating element, hot section, unetched polished specimen. Magnification = 50X.

Figure 5.6 is a micrograph of an etched polished specimen of the hot section. The dark areas are pores and the white areas are silicon carbide. The silicon carbide grains show the same dual phase, concentric structure as was found in the grains of the cold section. Quantitative x-ray analysis found the amount of α-silicon carbide to be 80,5% ($\pm$ 2,5%) and the amount of ß-silicon carbide to be 19,5% ($\pm$ 2,5%).

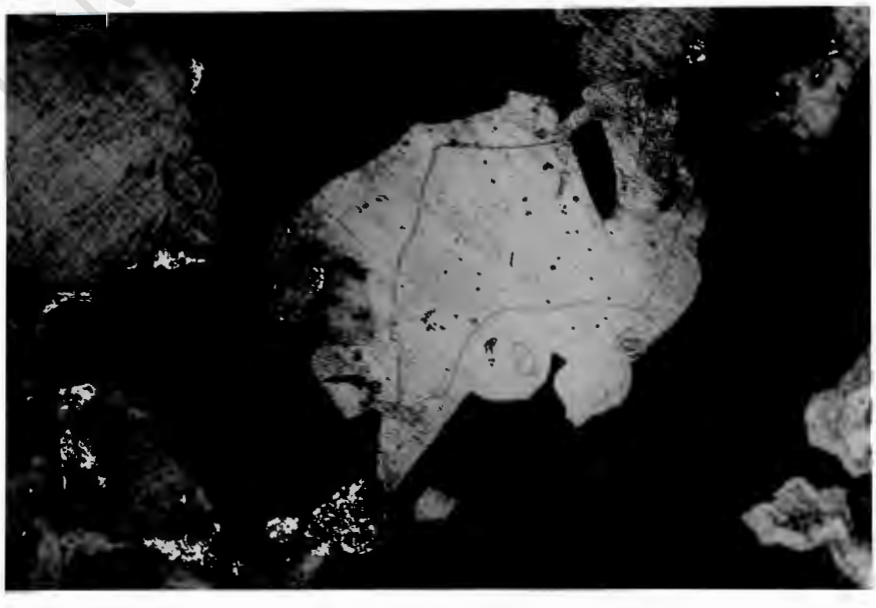

Figure 5.6: Kanthal Hot Rod heating element, hot section, etched polished specimen. Magnification = 110X.

It would appear that the concentric structure of the dual-phase silicon carbide grains found in this type of heating element has not been documented before. The starting powders used in the production of heating elements are practically pure green grade α-silicon carbide and thus the ß-phase must have been developed during the production of the heating elements. This structure is present in both the hot and cold sections. Furthermore, the ratio of the α- to ß-silicon carbide in the hot section (75:25) is similar to that found in the cold section (80:20). It is therefore clear that the outer layer of ß-silicon carbide was not formed as a result of siliconizing of the cold sections, but that it must have formed during the sintering stage. There are two possible explanations for the development of this dual phase structure:

a. The ß-silicon carbide was formed as a result of the evaporation-condensation sintering mechanism.

b. The α-silicon carbide converted to ß-silicon carbide during sintering.

It is unlikely that the mechanism of evaporation-condensation is the explanation for the dual phase structure. In such a process the smaller silicon carbide grains would evaporate and condense at the contacts between larger grains as ß-silicon carbide. However, Figure 5.3 shows that the smaller grains also have this dual phase structure.

Baumann, Jr. (1952) found that ß-silicon carbide is stable in an air atmosphere up to about 2100°C. ß-silicon carbide begins to transform monotropically to α-silicon carbide slowly at 2100°C, but at 2300°C the transformation is rapid and complete. However, Jepps and Page (1981) found that α-silicon carbide will convert back to ß-silicon carbide if heated in a nitrogen atmosphere, even at temperatures above 2100°C. Figure 5.7 shows the extent of the α- to ß-phase conversion at nitrogen pressures of 3 MPa and 0.1 MPa (atmospheric pressure) over the temperature range of 1800°C to 2500°C, as measured by them. The graph shows that the higher the temperature and the nitrogen pressure, the more α-silicon carbide converts to ß-silicon carbide.

The dual phase structure of the silicon carbide grains of the Kanthal Hot Rod heating element is thus the result of α- to ß-phase conversion during sintering in a nitrogen atmosphere.

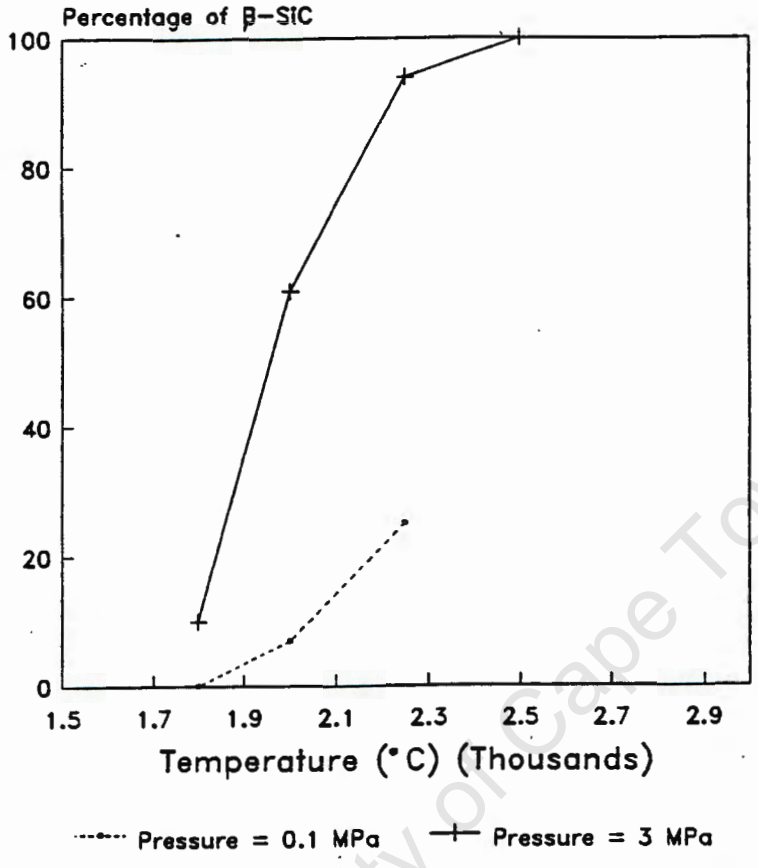

Figure 5.7: The percentage of α-silicon carbide that has converted to ß-silicon carbide in a nitrogen atmosphere. The samples were treated at pressures of 0.1 MPa and 3 MPa for a period of 30 minutes.

5.1.3 Fracture surfaces of Kanthal Hot Rod hot section before and after sintering

Scanning electron micrographs were taken of fracture surfaces of a Kanthal Hot Rod hot section, before and after sintering. Before sintering (Figures 5.8 and 5.9), the silicon carbide particles have sharp jagged edges and are loosely held together. The average lineal intercept length of the grains is 0.12 mm. Figures 5.10 and 5.11 show the Kanthal hot section after sintering. The micrographs show how the previously jagged edges of the silicon carbide particles are now rounded, while necking between a few of the particles can also be observed. There is no noticeable change in grain size.

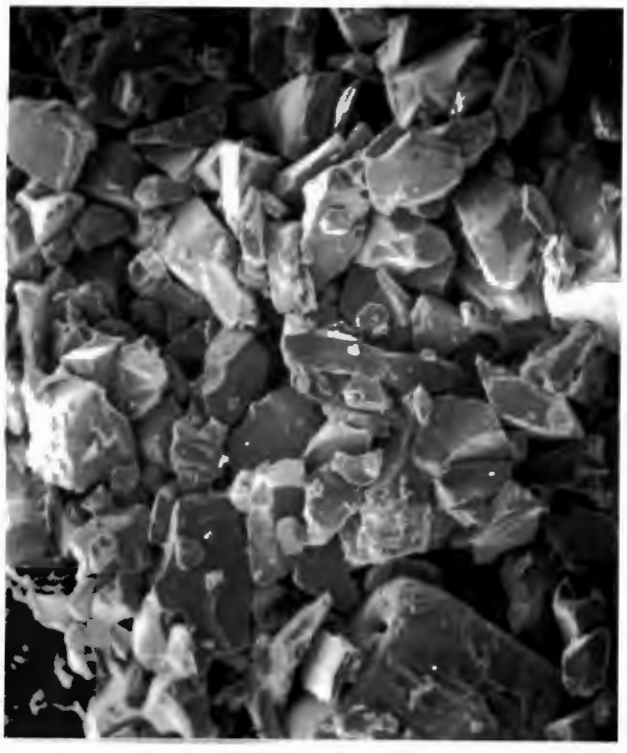

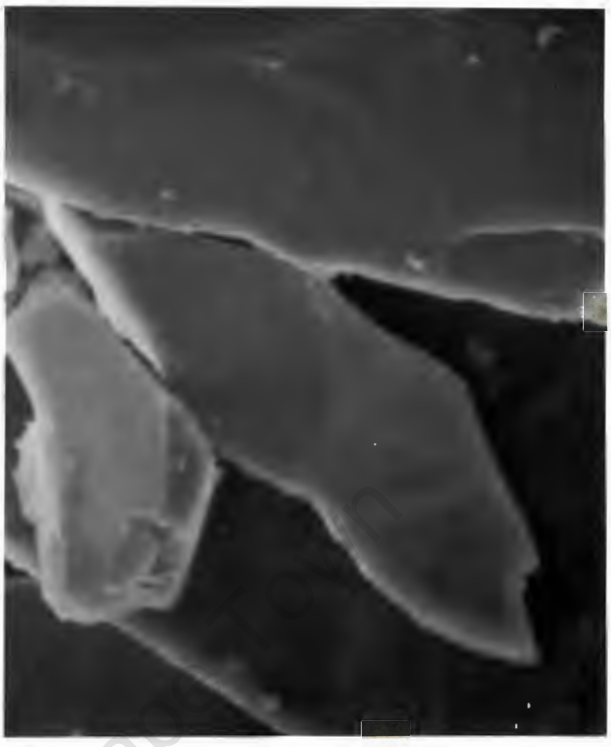

Figure 5.8 and Figure 5.9: Fracture surface of the hot section of a Kanthal Hot Rod heating element, before sintering. Magnification = 80X and 1250X.

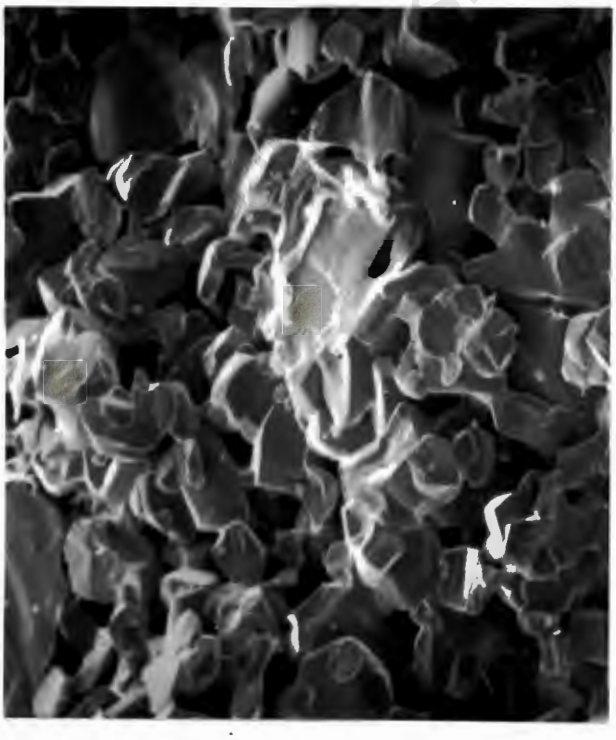

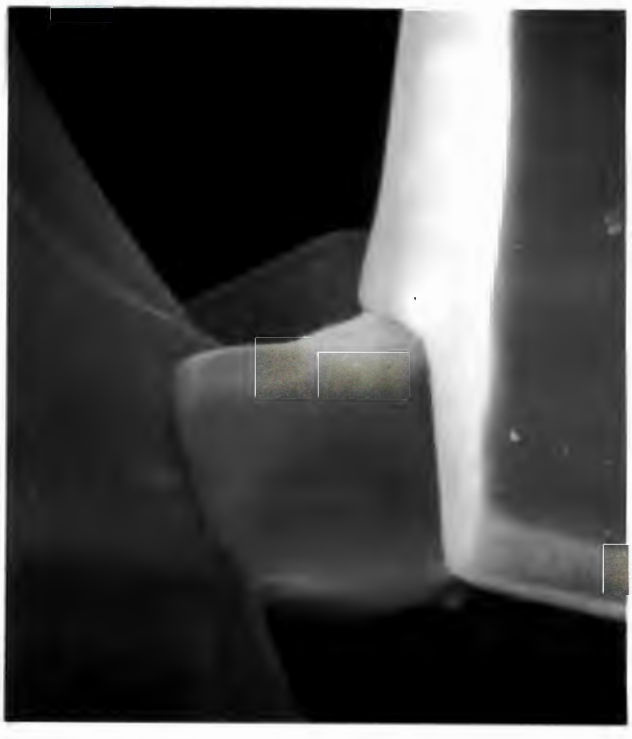

Figure 5.10 and Figure 5.11: Fracture surface of the hot section Kanthal Hot Rod heating element, after sintering. Magnification = 80X and 1250X.

5.2 Type 2: Carborundum heating element Type LL

The hot and cold sections of this type of heating element are manufactured separately. The hot section is produced from a selection of different α-silicon carbide grits, mixed with binders, water and a burn-out material, such as sawdust. This blend is then extruded into rods or packed into cardboard tubes and sintered at temperatures above 2200°C in a nitrogen atmosphere for about an hour. The sintering mechanism is evaporation-condensation. The cold section is produced by adding fine pure silicon metal and some carbon to the mix instead of the burn-out material. Sintering takes place by the reaction bonding mechanism. After sintering, the hot and cold sections are welded together, using a binding cement and high temperature localized heating.

5.2.1 Cold section

Figure 5.12 is a micrograph of an unetched polished specimen of the cold section. Free silicon is visible here as small bright white isolated areas and, from lineal analysis, constitutes about 3% of the structure. It was not possible to determine the amount of silicon present more accurately by x-ray diffraction because the amount present is too small to be measured sensibly. The black areas in the micrograph are pores and constitute 8.1% of this structure. The average pore intercept length is 0.04 mm.

Figure 5.12: Carborundum heating element Type LL, cold section, unetched polished specimen. Magnification = 110X.

Figure 5.13 shows an etched polished surface of the cold section. Lineal analysis indicated the ratio of fine to coarse grains to be approximately 80% to 20%. The average intercept length of the large grains is 0.136 mm and for the small grains it is 0.01 mm. The small amount of free silicon can not be seen in this micrograph.

The micrograph also shows that the larger grains have a similar dual phase structure to that found in the Kanthal heating element, although it appears that the outer concentric layer of the ß-phase is smaller than that found in the Kanthal heating element. X-ray diffraction analysis showed that the total amount of α- and ß-silicon carbide present was 53,5% (± 2,5%) and 46,5% (± 2,5%) respectively.

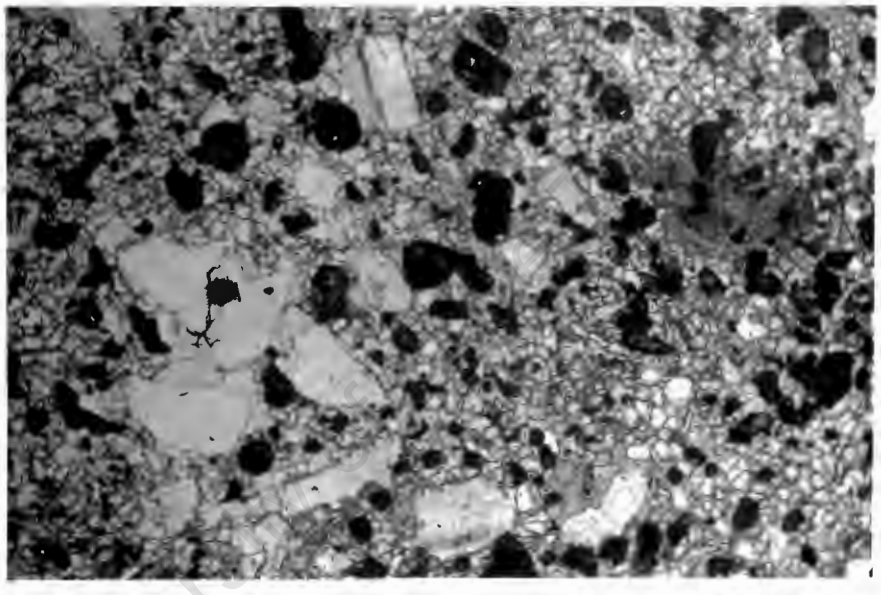

Figure 5.13: Carborundum heating element Type LL, cold section, etched polished specimen. Magnification = 110X.

Reaction bonded silicon carbide is formed by sintering a body consisting of free carbon, silicon and silicon carbide. The silicon reacts with the free carbon to form primary silicon carbide, which is always ß-silicon carbide (Baumann Jr., 1952 and Kriegesmann, 1988). If the sintering takes place in a nitrogen atmosphere the newly formed ß-phase is stabilized and will not convert to the α-phase (Jepps and Page, 1981). The surface of the large α-silicon carbide grains converts slowly to ß-silicon carbide and the grains show the same concentric structure as that found in the grains of the cold section of the Kanthal Hot Rod heating element. The formation of new silicon carbide by the reaction between carbon and silicon, plus the dual phase structure of the large grains, explains the high ß-silicon carbide content of this material.

A micrograph of a reaction bonded silicon carbide, taken by Wu et al (1985), shows the larger and smaller grains of that material to be similar in nature to those seen in Figure 5.13. However, a large amount of free silicon forms the matrix in Wu's material.

5.2.2 Hot section

Figure 5.14 is a micrograph of an unetched polished specimen of the hot section. Lineal analysis showed that silicon carbide constituted 63% of the structure and the pores 37%. The interconnected pore structure is very coarse, with large and rounded pores, which were probably produced as a result of the sawdust burning out. The average pore intercept length of the large pores is 0.46 mm and the average grain intercept length is 0.31 mm.

Figure 5.14: Carborundum heating element Type LL, hot section, unetched polished specimen. Magnification = 50X.

X-ray diffraction of the hot section showed the amount of α-silicon carbide to be 90,2% (±2,5%), thus the amount of ß-silicon carbide present is 9,8% (± 2,5%). Figure 5.15 shows an etched polished specimen of the hot section. The light areas are silicon carbide and the dark areas are pores. The silicon carbide phase appears to consist of grains that have sintered together very well. However, the dual phase structure is not as clearly developed, as in the Kanthal hot section material.

Figure 5.15: Carborundum heating element Type LL, hot section, etched polished specimen. Magnification = 110X.

The microstructure of the hot section is clearly very different to that of the cold section. The grains are much coarser and appear to have sintered to a high degree. Furthermore, there is also a virtual absence of a dual phase structure in the silicon carbide grains and only a relatively small amount of ß-silicon carbide present in this material, as compared to the Kanthal material.

5.3 Type 3: Kanthal Crusilite heating element

No manufacturing details for this type of element are available, but the Crusilite heating element is probably produced by a reaction-bonding process. The material consists essentially of ß-silicon carbide. The heating element is produced as a thin walled tube and the hot and cold sections consist of the same material. The hot section is made by mechanically cutting a spiral in the tube, thus increasing the electrical resistance of that section.

Figure 5.16 shows the microstructure of the Crusilite heating element. Quantitative x-ray analysis showed that the heating element consists only of ß-silicon carbide. The dark areas are pores and the lighter areas are silicon carbide. The pores are very small and evenly distributed with an average intercept length of 0.01 mm. Lineal analysis showed that the pores constitute 27% and the silicon carbide 73% of the structure. The hot and cold sections have identical microstructures.

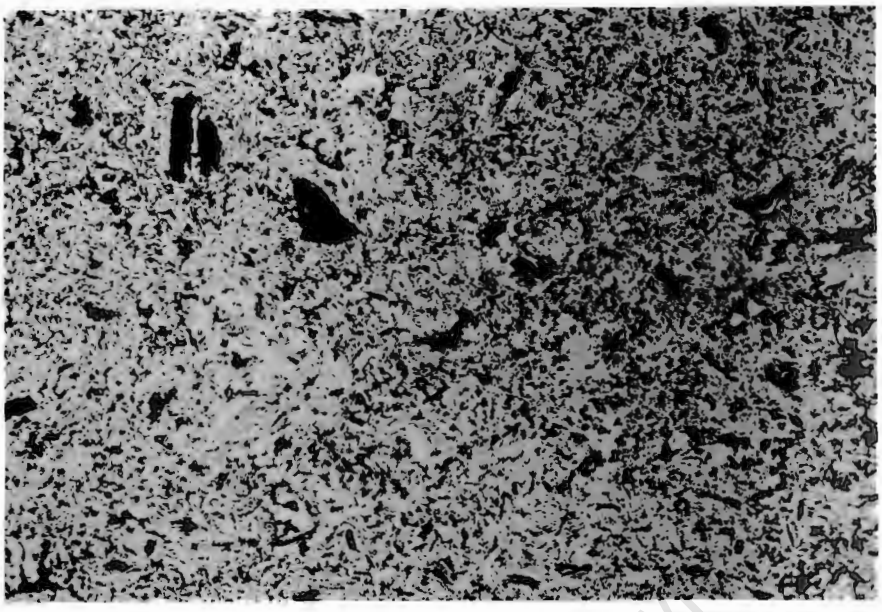

Figure 5.16: Kanthal Crusilite heating element, unetched polished specimen. Magnification = 110X.

5.4 Summary

Although all the heating elements are designed for similar operating conditions, there are significant differences in their microstructures. Table 5.1 compares average pore intercept lengths and average grain intercept lengths of the different heating elements, while Table 5.2 compares the percentage of pores, as well as the amount of α- and ß-silicon carbide and silicon present in the different heating elements.

Table 5.1: Comparison of the different pore and grain intercept lengths of different heating elements.

	Average pore intercept length (mm).	Average grain intercept length (mm).
Kanthal Hot Rod Cold section.	Completely infiltrated with silicon. Intercept length = 0.1	0.17
Kanthal Hot Rod Hot section	0.13	0.15
Carborundum Type LL Cold Section.	0.04	Two distinct grain sizes. Smaller size approx. 0.01 mm, larger size approx. 0.136 mm.
Carborundum Type LL Hot section.	0.46	0.31
Kanthal Crusilite.	0.01	(not measurable)

Table 5.2: Comparison of the percentage of pores, α- and ß-silicon carbide and silicon of the different heating elements.

	Pores (%)	Silicon (%)	α-SiC (%)	ß-SiC (%)
Kanthal Hot Rod Cold section.	-	45,0	41,0	14,0
Kanthal Hot Rod Hot section.	48,1	-	41,9	10,0
Carborundum Cold section.	8,1	3,0	47,6	41,3
Carborundum Hot section.	37,0	-	56.8	6.2
Kanthal Crusilite	27,0	-	-	73,0

The hot sections of both the Kanthal Hot Rod and the Carborundum Type LL heating element are produced by the evaporation-condensation mechanism. However, there are a few distinct differences between the two materials:

1. The pore size of the Carborundum material is considerably larger than that of the Kanthal material. These large pores are probably due to the relatively coarse sawdust which was added to the initial mix and which subsequently burnt out during sintering.

2. In comparison to the Kanthal material the α- to ß-phase transformation is lower in the Carborundum material. This could be due to one or a combination of the following differences in the sintering conditions used for the Carborundum process:

a. Shorter sintering times.
b. Lower nitrogen pressure in the furnace.
c. A lower sintering temperature.

6. EFFECT OF FABRICATION PARAMETERS ON THE RESISTIVITY OF SILICON CARBIDE

The understanding of the factors which influence the electrical resistivity of sintered silicon carbide is essential in the production of heating elements. The objective of this study was to determine the influence of fabrication parameters and physical properties upon the electrical resistivity of silicon carbide.

6.1 Relationship between density, sintering time and sintering temperature

The degree of sintering of each sample was dependent upon its particle size distribution and the sintering conditions. The samples obtained from Mixes 7, 8 and 9 had good green strength and sintered effectively, but all of the samples produced from Mix 1 were discarded because they had sintered very poorly. Figure 6.1 shows the relationship found between the density and the sintering conditions of Mixes 7, 8 and 9. Mixes 2 to 6 also showed similar trends and their results lay between those of Mixes 7 and 9. The average densities of each mix after sintering at 2200°C are listed in Table 6.1.

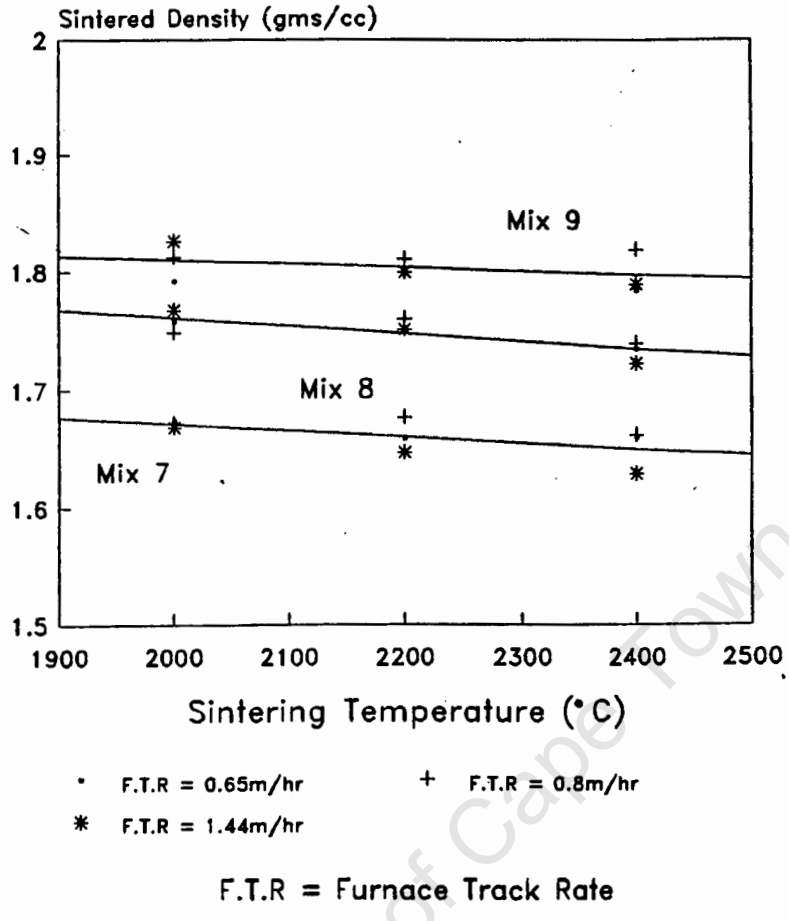

Figure 6.1: Density vs sintering temperature for Mixes 7, 8 and 9.

Table 6.1: Average density of each mix after sintering at 2200°C.

Mix	Density g/cc
2	1.84
3	1.82
4	1.79
5	1.76
6	1.76
7	1.66
8	1.75
9	1.80

It is clear from Figure 6.1 that the density of each sample was not dependent upon the sintering temperature or time. Densification did not occur because the sintering mechanism was evaporation-condensation. The slight decrease in density with increasing sintering temperature for some of the trends could not be explained. The differences in the sintered densities of the mixes are the result of differences in the packing densities of each mix. The correct blending of grits to control the packing density is thus very important.

6.1.2 Relationship between crushing strength and sintering temperature

Evaporation-condensation sintering results in bonding between individual silicon carbide particles in a sample without densification. The increase of the contact areas between the particles, due to material transfer by the evaporation-condensation mechanism, results in an increase in strength. The extent of sintering by evaporation-condensation is thus not reflected by an increase in density, but by the development of strength in the sintered material. Figure 6.2 shows the general trend between the sintering temperature and the crushing strength at a F.T.R of 0.80 m/hr for Mixes 7, 8 and 9. The results for only one track rate was plotted on the graph because there was little difference between the other track rates of 0.65 m/hr and 1.44 m/hr. There was a wide scatter between the data points and the relationship is not necessarily linear. Much more data would be required for a more exact analysis of the development of strength in terms of sintering time and temperature.

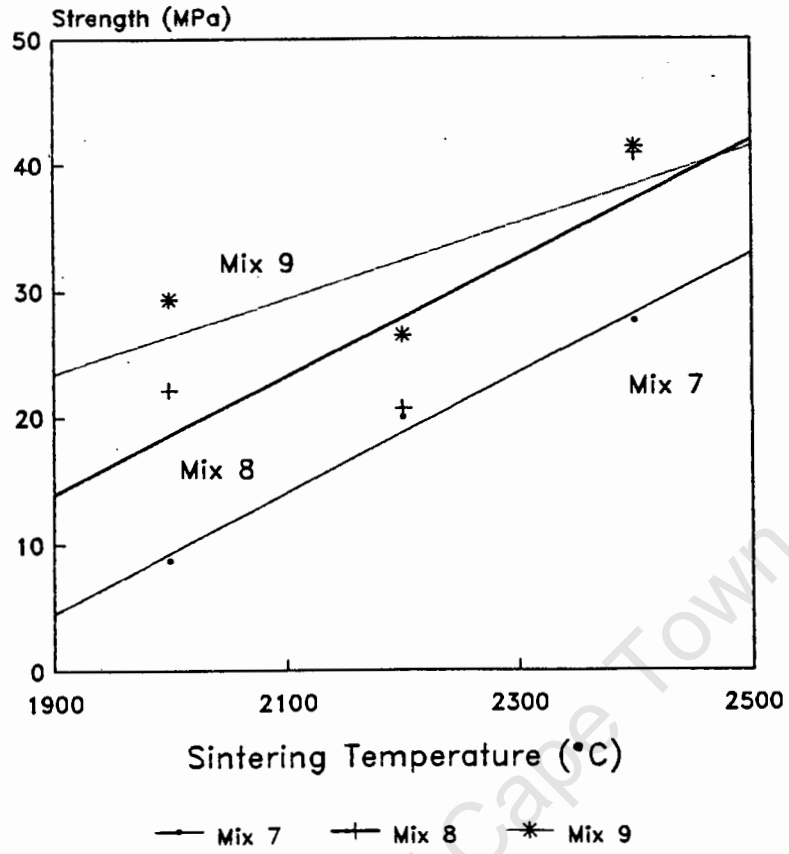

Figure 6.2: Crushing strength vs sintering temperature for Mixes 7, 8 and 9 at a F.T.R of 0.80 m/hr.

The above graph indicates that for each mix the crushing strength increases with increasing sintering temperature. Thus the higher the sintering temperature, the greater the extent of evaporation-condensation sintering, and the stronger the material.

6.1.3 Relationship between the sintered density and resistivity

Figure 6.3 shows the relationship between sintered density of the samples and their resistivity as measured at 800°C. The density of each mix remained relatively constant and lies on a horizontal line, as is clearly shown by Mix 7. However, there was a large variation in resistivity between the different mixes.

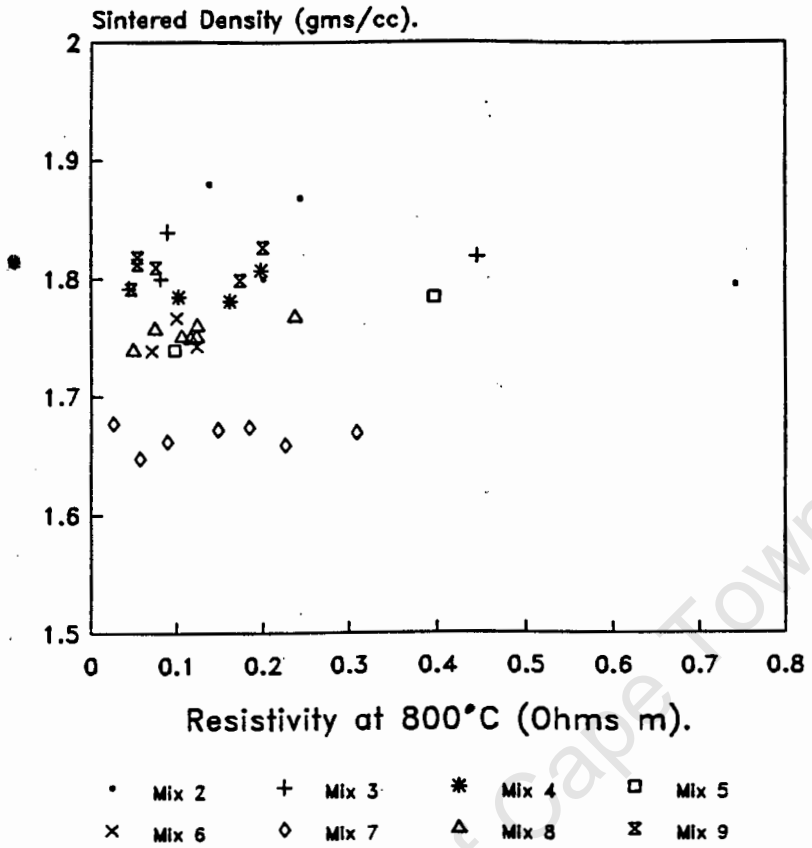

Figure 6.3: Sintered density vs resistivity at 800°C for Mixes 2 to 9.

6.1.4 Relationship between the crushing strength and resistivity at 800°C

The improved contact between the particles due to sintering reduces the resistivity of the material. Therefore, the greater the strength of the material the lower its resistivity. This relationship, shown in Figure 6.4, appears not to be linear. The relatively large scatter in the data points is mainly due to the poor reproducibility of the crushing strength measurements.

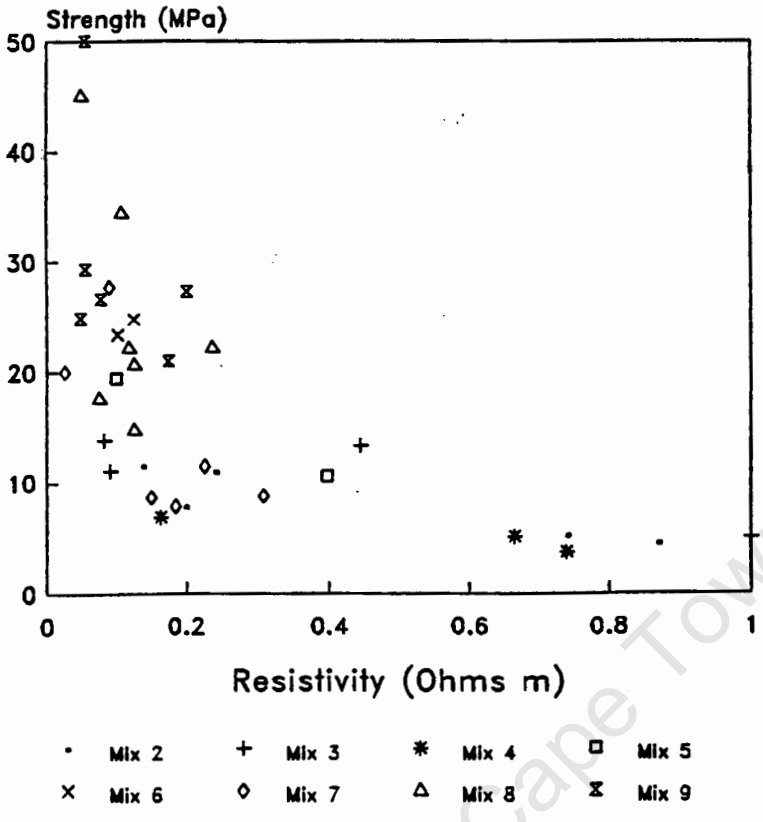

Figure 6.4: Crushing strength vs resistivity at 800°C of Mixes 2 to 9.

6.2 Summary

The results of the study only give an indication of general trends and much more data would be required for a more detailed analysis.

Table 6.2 compares the results of Mixes 7, 8 and 9. The F.T.R and the sintering time chosen for the comparison were 0.8 m/hr and 2000°C respectively. For a comparison, the resistivity, density and strength of the hot section of a Kanthal Hot Rod were measured. The resistivity of the heating element was substantially lower than that of the laboratory samples, while the crushing strength was substantially higher. The high strength and the low resistivity of the heating element agrees with the results shown by Figure 6.4. The density of the heating element was also substantially higher than the densities found for the different mixes.

Table 6.2: Results of the Kanthal hot section Hot Rod heating element and Mixes 7, 8 and 9 at 2000°C at a F.T.R of 0.8 m/hr.

	Kanthal Hot Rod	Mix 7	Mix 8	Mix 9
Sintered Density (g/cc)	2,19	1,67	1,75	1,81
Crushing Strength (MPa)(approx.)	60,0	8,7	22,2	29,3
Resistivity (Ωm)	0,004	0,148	0,120	0,054

The study revealed that the resistivity of silicon carbide heating elements is strongly dependent on their density. Because sintering does not lead to densification, the high density required must be achieved in the green state by controlling the packing density. It would appear that the packing densities achieved with the laboratory mixes were not high enough and further work would be needed to improve this aspect of fabrication.

Resistivity is also dependent on the sintering conditions, therefore it would be necessary to determine the relationship between sintering temperature and sintering time (F.T.R) for each specific fabrication facility, in order to establish the conditions for optimum economic and technical production.

7. REFERENCES

ALLIEGRO, R., COFFIN, L. and TINKLEPAUGH, J. (1956): "Pressure - sintered silicon carbide". *J. Amer. Ceram. Soc.*, 39, 386-389.

BAUMANN, H. (jnr.) (1952): "The relationship of alpha and beta silicon carbide". *J. Elect. Chem. Soc.*, 99, 109-144.

BERROTH, K. E. (1990): "Silicon carbide materials for high duty seal applications". *Ingenieurkeramik Schunk* - Dyko, Dusseldorf, West Germany.

BIND, J. N. and BIGGERS, J. V. (1975): "Hot pressing of silicon carbide with 1% boron carbide addition". *J. Am. Ceram. Soc.* 58, 304-306.

BIND, J. (1977): Penn State University, University Park, Pennsylvania, U. S. A. JCPS Grant in Aid Report.

CLINTON, D. J. (1987): "A guide to polishing and etching of technical and engineering ceramics". The Institute of Ceramics, Stoke-on-Trent.

COES, L. (1971): "Abrasives". *Springer-Verlag.*, New York, Wein.

COPPOLA, A. and McMURTRY, C. (1976): "Substitution of ceramics of ductile materials in design". *Proceedings of the National Symposium on Ceramics in Service of Man.* Carnegie Institute, Washington DC.

ESK (1988): "Engineered ceramics for the chemical industry". Brochure kindly supplied by *Elektroschmelzwerk Kempten GMBH.*

FORREST, C. W., KENNEDY, P.M. and SHENNAN, J. V. (1972): "The fabrication and properties of self bonded silicon carbide bodies". *Special Ceramics 5.* Proceedings of the fifth symposium on Special Ceramics held by The British Ceramic Research Association. Ed: Popper, p. 99-124.

HANNAM, A. L. and SHAFFER, P. T. B. (1969): "Revised x-ray diffraction line intensities for silicon carbide polytypes". *J. Appl. Cryst.*, 2,45.

HEUER, A. H., FRYBURG, G. A., OGBUJI L. U. and MITCHELL, T. E. (1978): "ß to α transformation in polycrystalline SiC: I, microstructural aspects". *J. Am. Ceram. Soc.*, 61, [9], 406-412.

JEPPS, N. W. and PAGE, T. F. (1981): "The 6H to 3C 'reverse' transformation in silicon carbide compacts". *J. Amer. Cer. Soc.*, 64, (12), C177-178.

KANTHAL (1989): "Kanthal silicon carbide electric heating elements". Kanthal brochure.

KRIEGESMANN, J. (1986): "Sintering phenomena in silicon carbide". *Powder Metallurgy International*, 18, (5), 341-343.

KRIEGESMANN, J. (1988): "Competing sintering mechanisms in silicon carbide". *Advanced Ceramics.*, Interceram 2, 27-30.

LANGE, F. F. and ISKOE, J. L. (1974): "High temperature strength behavior of hot pressed Si_3N_4 and SiC; effect of impurities". *Ceramics for High Performance Applications*, Eds: Burke, H. Gorum, A. and Katz, K. Metals and Ceramics Information Center, Columbus, OH, 223-38.

LEITHSCHMIDT, K. (1982): "Siliciumcarbid". In: K. Winnacker und L. Kuchler (Hsgb.) *Chemische Technologie*, Band 2, Anorg. Techn. 1, 4. Auflage, Hanser-Verlag, 626-629.

LASHWAY, R. A., SESHADRI, S. G. and SRINIVASAN, M. (1984): "Various forms of silicon carbide and their effects on seal performance". *Lubrication Engineering*. 40, (6), 356-363. Carborundum Resistant Materials Company, Niagara Falls, NY 14302.

LAUBSCHER, N. F. (1965): "Testing Outlying Observations". National Physical Research Laboratory, South African Council for Scientific and Industrial Research, Pretoria.

MILLER, R. J. (1966): "Regression techniques". *Simultaneous statistical inference.* Eds. McGraw-Hill, Inc.

NADEAU, J. S. (1973): "Very high pressure hot pressing of silicon carbide". *Amer. Ceram. Soc. Bull.*, 52 [2] 170-76.

NESS, J. N. and PAGE, T. F. (1986): "Microstructural evolution in reaction bonded silicon carbide". *J. Mat. Sci.* 21, 1093-2216.

PAULING, L. (1960): *Nature of the Chemical Bond.* Cornel University Press, Ithaca, New York, 3rd Ed., p98.

PROCHAZCA, S. (1974): "Sintering of Silicon Carbide". *Ceramics for High Performance Applications.* Eds: Burke, H. Gorum, A. and Katz, K. Metals and Ceramics Information Center, Columbus, OH.

PROCHAZCA, S. (1975): "The role of boron and carbon in sintering of silicon carbide". *Proceedings on the Conference on Special Ceramics*, Ed: Popper, P., British Ceramic Research Association, 6, 171-84.

PROCHAZCA, S. and CHARLES, R. J. (1973): "Strength of boron-doped, hot-pressed silicon carbide". *Am. Ceram. Soc. Bull.* 52, 885-891.

RAMSDELL, L.S. (1947): "Studies on silicon carbide". *Am. Min.*, 32, 64-81.

SCHWETZ, K. A. (1989): "Silicon carbide and its high-technology ceramics". Sonderdruck Aus, 'Radex-Rundschau', Heft 1, 1989, Radex Austria A. G. Fur Feuerfeeste Erzeugnisse, Radenthein/Karnten.

SUNIL DUTTA (1984): "Sinterability, strength and oxidation of alpha silicon carbide powders". *J. Mat. Sci.*, 19, 1307-1313.

SUNIL DUTTA (1985): "Densification and properties of alpha silicon carbide". *J. Am. Ceram. Soc.*, 68 [10] C-269 - C-270.

SUNIL DUTTA (1988): "Improved processing of alpha-SiC". *Adv. Ceram. Mat.*, 3, [3], 257-62. Lewis Research Center, Cleveland, OH 44135

THIBAULT, N. W. (1944): "Morphological and structural crystallography and optical properties of silicon carbide". *Am. Mineral.*, 29, 249-278.

WATSON, G. K., MOORE, T. J. and MILLARD, M. L. (1985): "Effect of hot isostatic pressing on the properties of sintered alpha silicon carbide". *Am. Ceram. Soc. Bull.*, 64 [9], 1253-56.

WHALLEN, T. J. (1986): "Processing and properties of structural silicon carbide". *Ceramic Engineering and Science Proceedings*, 7, 1135-1143. Research Staff, Ford Motor Company, Dearborn, MI 48121,

WU, C. C., RICE, R. W., PLATT, B. A. and CARRLE, S. (1985): "Wear and microstructure of SiC ceramics". *Ceram. Eng. & Sci. Proc.*, 6, 1023-1039.

8. APPENDIX A1: QUANTITATIVE X-RAY DIFFRACTION OF SILICON CARBIDE MIXTURES

A quantitative diffraction technique, based on the intensity ratios of particular diffraction peaks of the spectra, was developed to estimate the relative amounts of the α- and ß-phases of silicon carbide in mixtures of these two phases.

A1.1 Equipment

The equipment used was a Philips PW 1400 diffraction spectrometer. Diffraction intensity data was collected digitally using the available communication software (COLLECT.EXE). The instrumental conditions used for recording the spectra were:

Radiation:	Cu Kα, 40 kV, 30 mA.
Receiving slit:	1°
Divergent slit:	1°
Step size:	0,1° 2-theta.
Count Time:	4 Seconds.
Angle sector:	28°-92° (2-theta)

A1.2 Standards

Powders of high purity α- and ß-SiC were obtained from the company Hermann C. Starck, Berlin. The properties of the powders (α-SiC labeled as A10 and ß-SiC labeled as B10) are listed in Table A1.

Table A1: Characteristics of α- and ß-SiC powders from Hermann C. Starck, Berlin.

	Units	*α-SiC (A10)*	*ß-SiC (B10)*
Powder Characteristics:			
Bet Specific Surface Area	m^2/g	13-17	13-17
FSSS Particle size (max.)	µm	0,8	0,8
Apparent Density	g/cc	,35-,55	,35-,55
Tap Density	g/cc	,55-,75	,55-,75
Phases (in mass %):			
α-SiC (6H structure) (min.)		97,5	
ß-SiC (min.)			97,5
Free silicon		0,1	0,1
Chemical Composition (in mass %):			
Nonmetallic Constituents:			
C		30-30,5	30-30,5
O (max.)		0,6	0,6
N (approx.)		0,03	0,04
F (approx.)		0,13	0,12
Metallic Impurities:			
Fe (max.)		0,05	0,05
Al (max.)		0,1	0,1
Ca (max.)		0,02	0,02
W (max.)		0,02	0,03

A1.3: X-ray diffraction pattern of silicon carbide

Figures A1 and A2 show the x-ray diffraction traces for α- and ß-SiC respectively, obtained from analysis of the standard powders. The d-values, relative intensities and Miller indices of the two compounds are listed in Table A2. The relative intensities were estimated from the counts at the peak maxima.

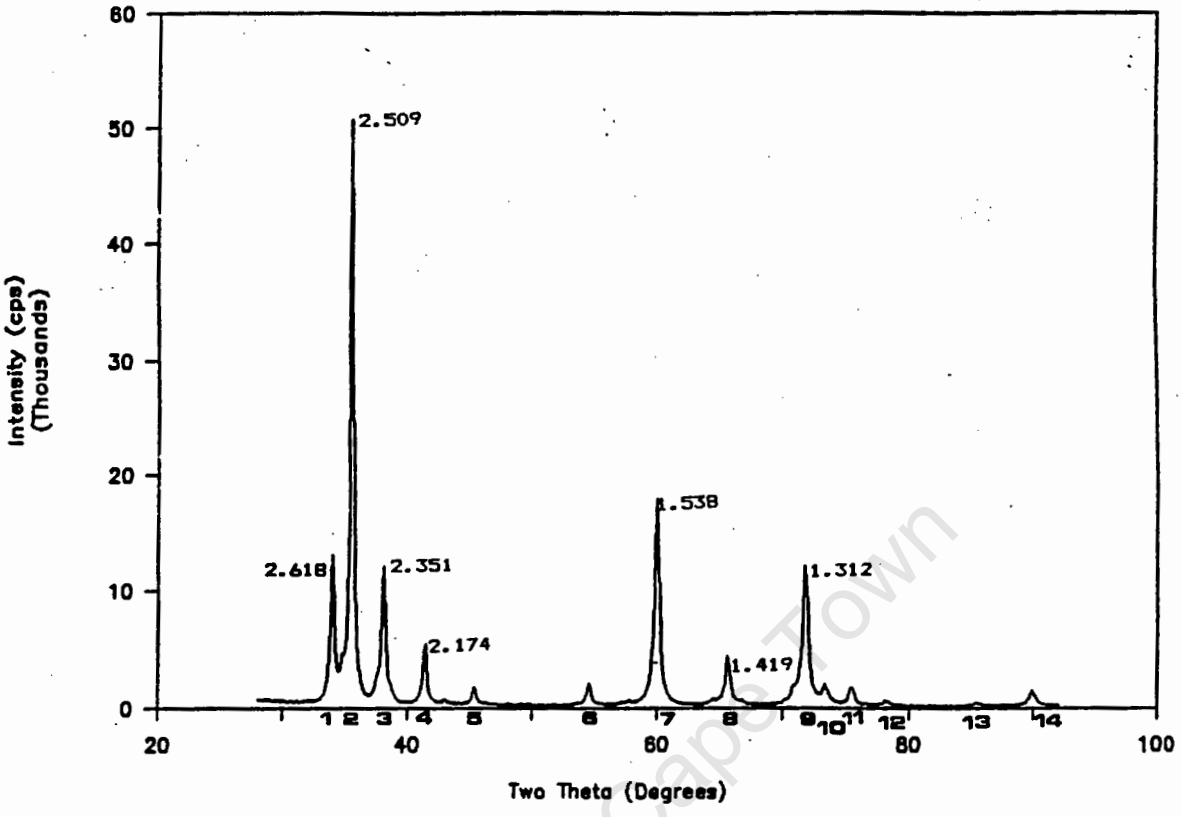

Figure A1: X-ray diffraction trace for α-SiC: Starck, A10.

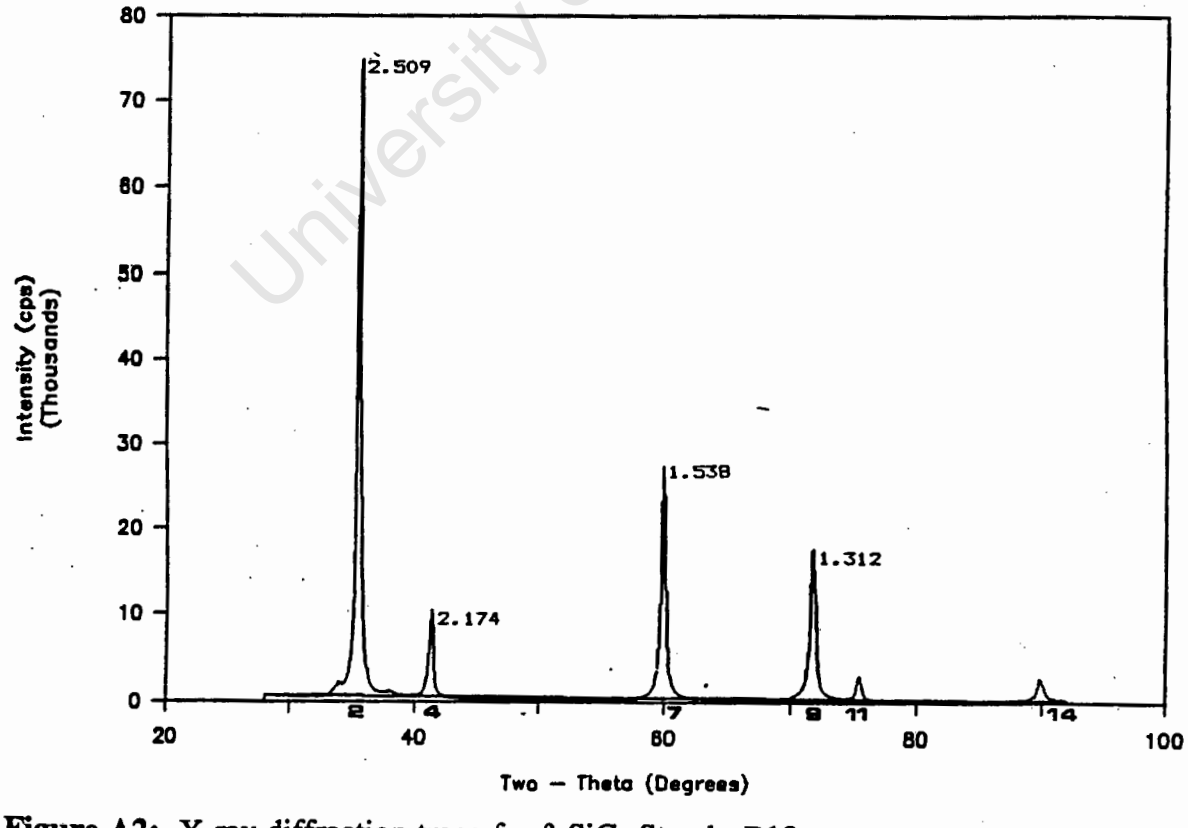

Figure A2: X-ray diffraction trace for ß-SiC: Starck, B10.

Table A2: Details of x-ray diffraction peaks of α- and ß-SiC.

	Peak Number	d value	Relative Intensities %	Miller Indices
α-SiC: (A10)	1	2,618	30	[101]
	2	2,509	100	[102]
	3	2,351	26	[103]
	4	2,174	10	[104]
	7	1,538	35	[108]
	8	1,419	9	[109]
	9	1,312	22	[10,10]
ß-SiC: (B10)	2	2,509	100	[111]
	4	2,174	13	[200]
	7	1,538	37	[220]
	9	1,312	24	[311]

It can clearly be seen that there are diffraction peaks that are common to both α- and ß-SiC and some peaks which occur only in the α-SiC spectrum. Unfortunately, there are no diffraction peaks which occur only in the ß-SiC spectrum. The ratio of intensities of the peaks common to both spectra (peaks 2, 4, 7, and 9) are similar, whether they are in the α- or ß-SiC spectrum.

The Miller indices for the spectrum of α-SiC were established by Hannam and Shaffer (1969) and relate to 4H, 6H and 15R structures. The data listed by Bind (1977) was used for the ß-SiC spectrum. According to Hannam and Shaffer (1969) peaks 2, 7 and 9 of the α-SiC spectrum are each due to several crystallographic planes (see Table A3), but with such small differences in d-spacing that they are not normally resolved.

Table A3: Composite diffraction peaks of α-SiC.

	d-spacing (Å)	Miller indices
Peak 2:	2,513	[006]
	2,509	[102]
Peak 7:	1,538	[108]
	1,536	[110]
Peak 9:	1,312	[10,10]
	1,311	[116]
	1,310	[202]

A1.4 Selection of peaks

In this work the usefulness of three peak intensity ratios for the quantitative determination of mixtures of α- and ß-silicon carbide were evaluated. The ratios are:

$$\text{Ratio 1} = \frac{\text{Peak 3 - Peak 4}}{\text{Peak 4}}$$

$$\text{Ratio 2} = \frac{\text{Peak 8 - Peak 7}}{\text{Peak 7}}$$

$$\text{Ratio 3} = \frac{\text{Peak 3 - Peak 2}}{\text{Peak 2}}$$

Ratio 3 uses peaks numbered 2 and 3 and was proposed by Baumann Jnr. (1952) for the quantitative analysis of mixtures of α- and ß-SiC. Peak 2 is common to both α- and ß-SiC while peak 3 is due to α-SiC only. Although peak 2 is the most intense and would normally be used, the poor background situation acts against it. As can be seen from Figure A1, the close proximity of other peaks, particularly peak 1, makes the determination of the background of peak 2 uncertain.

A1.5 Determination of the peak intensities and intensity ratios

From the data printout of the x-ray diffractometer the total intensities of the relevant peaks were determined by summing the counts between the following angles:

Peak 2:	34,8° - 36,9°
Peak 3:	37,0° - 39,6°
Peak 4:	40,5° - 42,5°
Peak 7:	58,7° - 61,2°
Peak 8:	64,1° - 67,0°

To find the net intensity of each peak, its background count had to be subtracted. The total background count was found by adding the count at the beginning and end of each peak, dividing by 2 and then multiplying by the number of steps recorded over each peak. For example, the intensity of peak 2 was calculated from the relevant portion of the diffraction data printout as follows:

Angle	Count	Angle	Count
34,8	2128	35,9	3414
34,9	2276	36,0	2134
35,0	2115	36,1	1459
35,1	2416	36,2	1164
35,2	3248	36,3	949
35,3	4997	36,4	723
35,4	9231	36,5	601
35,5	18405	36,6	602
35,6	21511	36,7	544
35,7	12929	36,8	479
35,8	5741	36,9	489

Total intensity: Sum of counts at all steps from 34,8° to 36,9° = 97555 counts.

Background intensity:

$$\frac{(\text{counts at } 34{,}8° + \text{counts at } 36{,}9°) * \text{Number of steps.}}{2}$$

$$= \frac{(2128 + 489) * 22}{2} = 28787 \text{ counts.}$$

Net intensity: 97555 - 28787 = 68768 counts

A1.6 Calibration curves

Mixtures of the α- and ß-SiC powders, over the full compositional range and with 10% step composition intervals were prepared. Each mix was homogenized by grinding for three minutes in a Siebtechnik crushing mill (Type T250). The three intensity ratios were determined from the diffraction spectra of each mixture and are listed in Table A4.

Table A4: Intensity ratios for mixtures of α- and ß-SiC.

Amount of α-SiC in the mixture (%)	Ratio 1	Ratio 2	Ratio 3
0	-0,999	-0,994	-0,998
10	-0,778	-0,958	-0,968
20	-0,608	-0,941	-0,946
30	-0,419	-0,928	-0,920
40	-0,216	-0,905	-0,889
50	0,021	-0,882	-0,862
60	0,410	-0,827	-0,815
70	0,782	-0,827	-0,775
80	1,203	-0,787	-0,722
90	1,716	-0,773	-0,652
100	2,342	-0,721	-0,663

To estimate the experimental errors, the pure α-SiC powder (A10) was scanned eleven times and ratios 1, 2 and 3 calculated. The outlying observations for each ratio were found (Laubscher, 1965). After excluding the outliers, the mean and standard deviations were calculated for each ratio (Table A5).

Table A5: Mean and standard deviations for Ratio 1, 2 and 3 for 100% α-SiC.

	Ratio 1	Ratio 2	Ratio 3
Mean Value	2,306	-0,7207	-0,6021
Standard Deviation (σ)	0,0411	0,0075	0,0233

Although the standard deviation of Ratio 2 is the smallest value it does not take into consideration the spread of the values on the y axis or the least squares (R^2) values.

Graphs were plotted of each ratio against the percentage of α-SiC present. Figure A3 is the graph of Ratio 1 versus percentage of α-SiC. The graph produces a non-linear curve. If a factor of 2 is added to Ratio 1 the curve corresponds to a logarithmic curve. The integer was added because it is not possible to take a logarithm of a negative or zero value. A straight line graph is achieved by taking the natural logarithm of this value and plotting it on the y axis (Figure A4).

Ratio 2 and Ratio 3 were also plotted against percentage of α-SiC and straight lines were found to fit best (Figure A5 and Figure A6). Statgraphics also provides the

statistical information for each graph (Table A6, A7, and A8). The several runs made to find the standard deviation of pure α-SiC was also plotted on each graph.

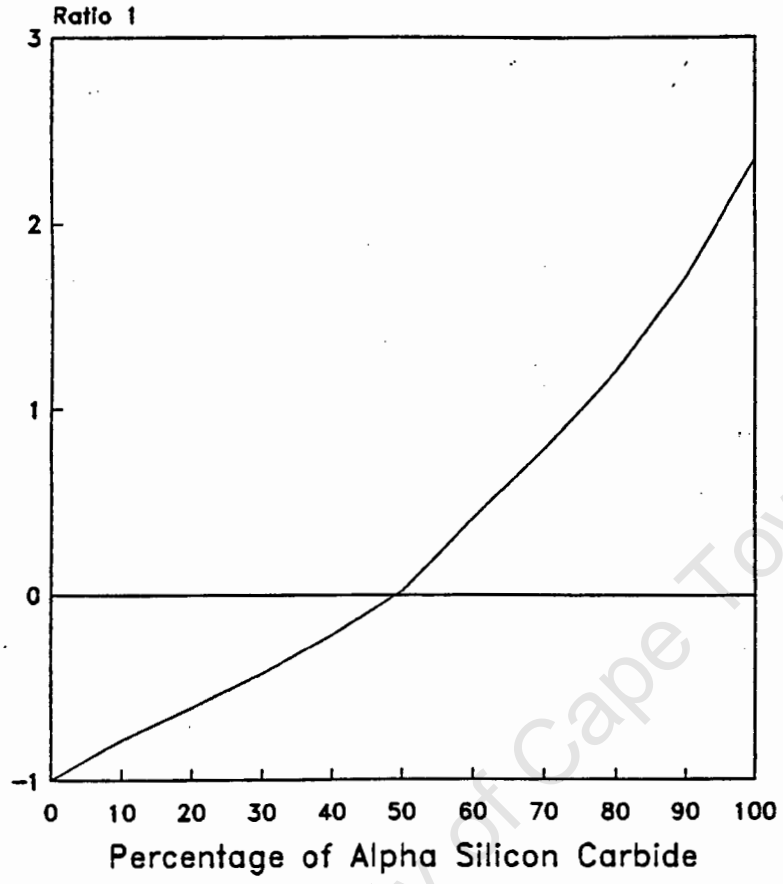

Figure A3: Ratio 1 vs % of α-SiC.

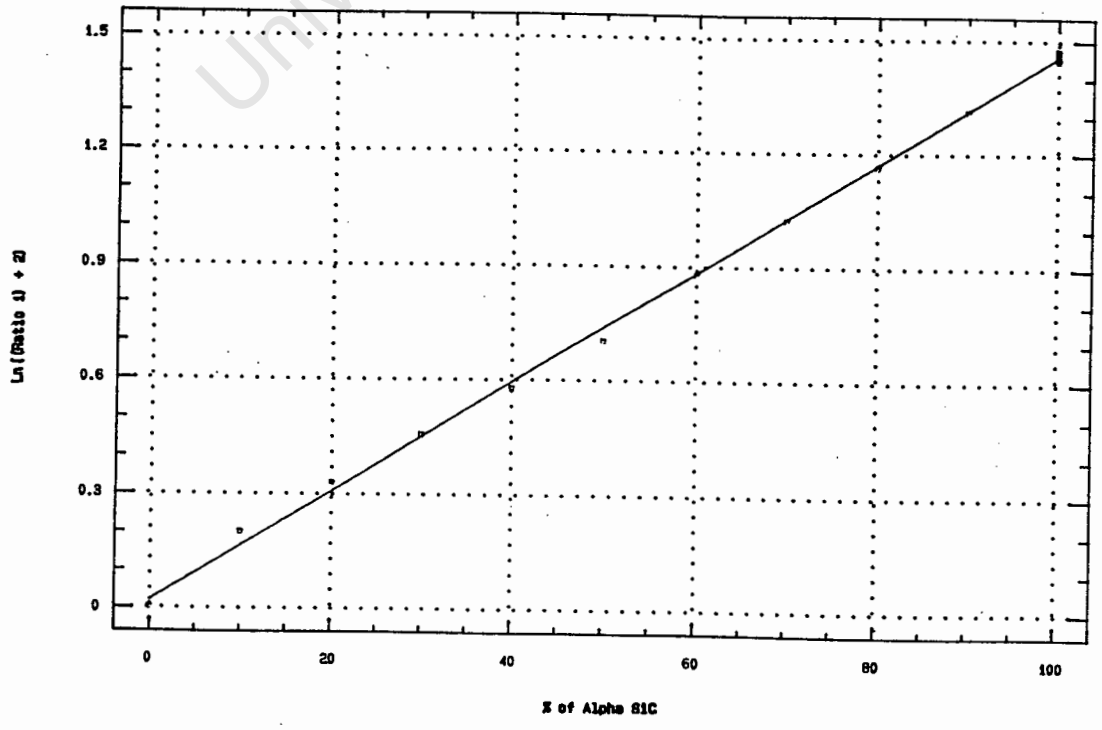

Figure A4: Ln((Ratio 1) + 2) vs % of α-SiC.

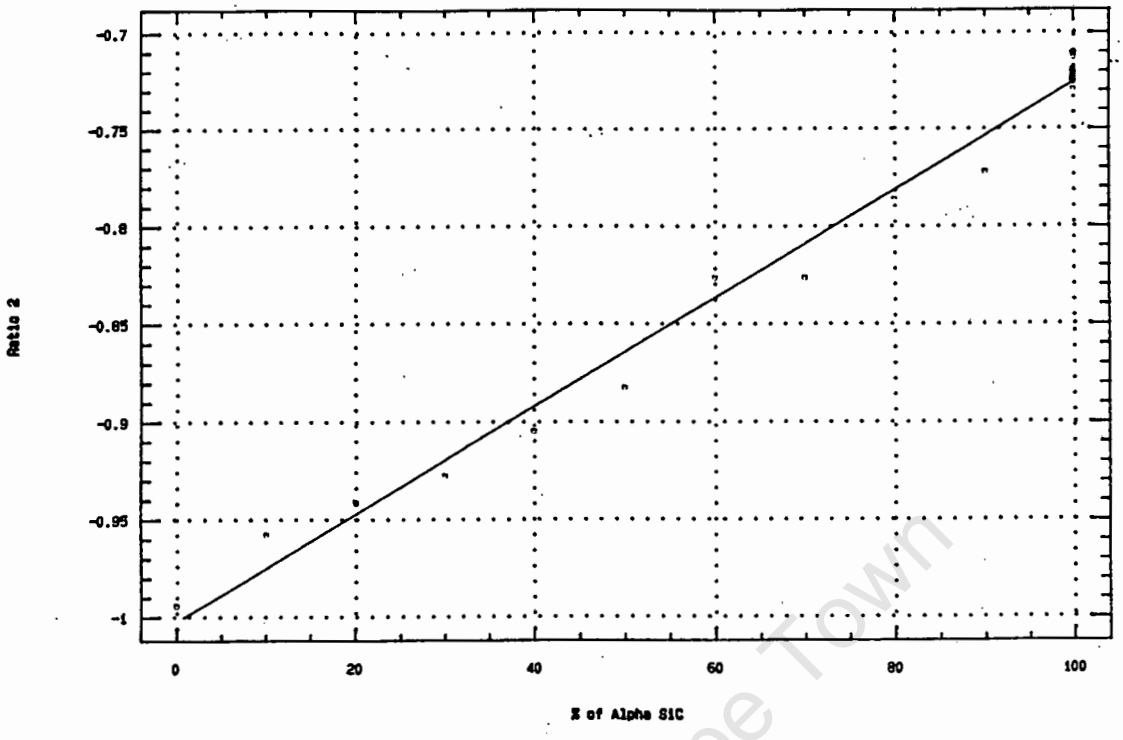

Figure A5: Ratio 2 vs % of α-silicon carbide.

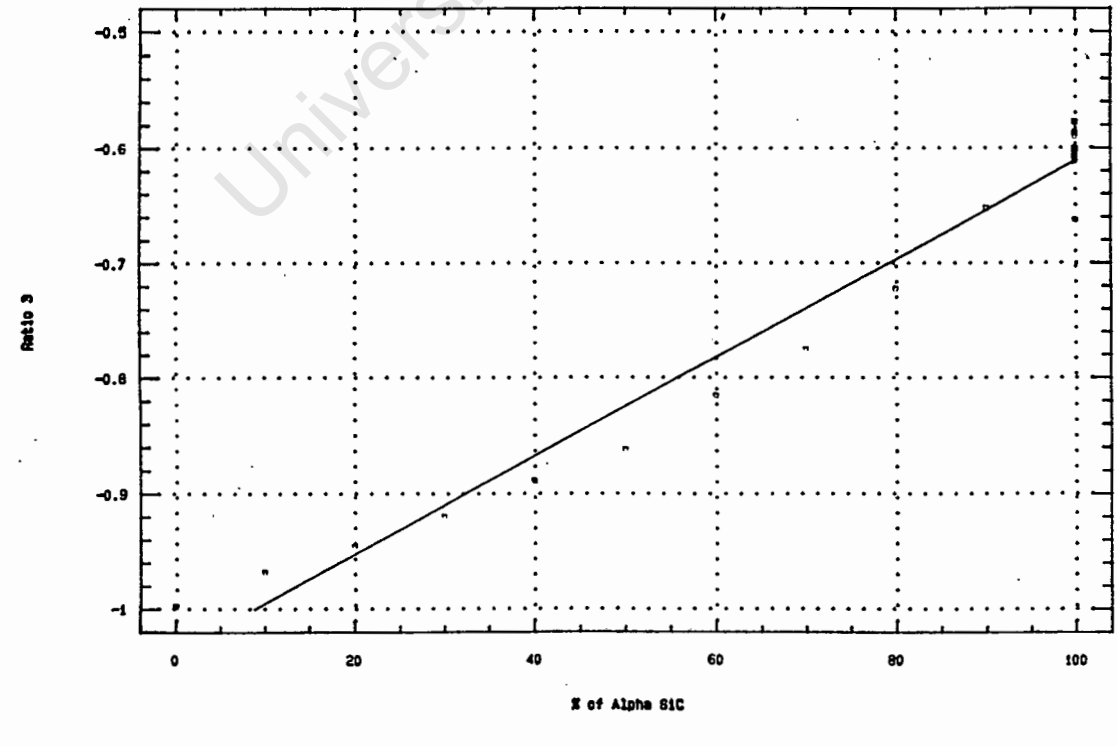

Figure A6: Ratio 3 vs % of α-SiC.

Table A6: Statistical information for the graph of Ratio 1 vs % of α-SiC (Figure A4).

Parameter	Estimate	Standard Error	T Value	Prob Level
Intercept	0,0212	8,79E-3	2,42	0,027
Slope	0,0144	1,11E-4	129,2	0,000
	Analysis of Variance			
Source	Sum of Squares	Df	Mean Square	F-Ratio	Prob. Level
Model	4,666	1	4,666	16693	0,000
Error	0,0047	17	0,00028		
Total (Corr.)	4,671	18			
R-squared = 99,90%					

Table A7: Statistical information for the graph of Ratio 2 vs % of α-SiC (Figure A5).

Parameter	Estimate	Standard Error	T Value	Prob Level
Intercept	-1,0023	6,04E-3	-165,90	0,000
Slope	2,765E-3	7,65E-5	36,1	0,000
	Analysis of Variance			
Source	Sum of Squares	Df	Mean Square	F-Ratio	Prob. Level
Model	0,173	1	0,1726	1306	0,000
Error	0,0022	17	0,00013		
Total (Corr.)	0,175	18			
R-squared = 98,72%					

Table A8: Statistical information for the graph of Ratio 3 vs % of α-SiC (Figure A6).

Parameter	Estimate	Standard Error	T Value	Prob Level
Intercept	-1,0375	0,01	71,718	0,000
Slope	4,26E-3	1,80E-4	23,6	0,000
	Analysis of Variance			
Source	Sum of Squares	Df	Mean Square	F-Ratio	Prob. Level
Model	0,425	1	0,425	558	0,000
Error	0,0137	18	0,00076		
Total (Corr.)	0,439	19			
R-squared = 96,87%					

A1.7 Establishing which intensity ratio gives the most accurate predictions for the % of α-silicon carbide

Fiellers' equation (or Paulsons') enables X (% of α-SiC) to be calculated from a known Y (Ratio 2 or Ratio 3) value (Miller, 1966). The equation can be used to find the percentage of α-SiC within 95% confidence limits. To find the percentage of α-SiC using Ratio 1, an integer of 2 must be added and then the natural logarithm taken of this value. These values can then substituted into Fiellers' equation and the percentage of α-SiC estimated.

In section A1.6 the mean and standard deviation were calculated for each ratio of pure α-SiC. The upper and lower limits of the Ratios are given in Table A9.

Table A9: The upper and lower limits calculated for Ratios 1, 2 and 3 at 100% α-SiC.

	Lower limit Mean + σ	Upper limit Mean - σ
Ratio 1	2,3471	2,2649
Ratio 2	-0,7132	-0,7282
Ratio 3	-0,5788	-0,6254

Using Fiellers' equation the percentage of α-SiC was determined in the pure α-SiC sample. The ratio which gives the smallest percentage difference between its upper and lower limits would be the better ratio to use for calculating the percentage of α-SiC. Table A10 shows the values calculated for Ratios 1, 2 and 3.

Table A10: Comparison of percentages found for Ratio 1, 2 and 3 for pure α-SiC.

	Ratio 1	Ratio 2	Ratio 3
Upper limit %	100,5 ± 2,5	105 ± 9	132 ± 15
Lower limit %	99,5 ± 2,5	99 ± 9	121 ± 15
Differences between lower and upper limits %	2	6	11

From the above Table the differences between the lower and upper limits and the spread of percentage values found for each ratio show that Ratio 1 is most favourable. The findings also show that Ratio 3 has a large error and is least favourable. Therefore, to find the percentage of α-SiC in a material by x-ray diffraction Ratio 1 would give the most acceptable results. This agrees with the least squares (R^2) values found for the graph of each Ratio (see Tables A6, A7, and A8).